https://doi.org/10.5194/nhess-2022-275
Preprint. Discussion started: 6 January 2023

Natural Hazards and Earth System Sciences
Discussions

A new modelling framework for regional assessment of extreme sea levels and associated coastal flooding along the German Baltic Sea coast

Joshua Kiesel[1], Marvin Lorenz[2], Marcel König[3], Ulf Gräwe[2], and Athanasios T. Vafeidis[1]

[1]Department of Geography, Christian-Albrechts-Universität zu Kiel, 24118, Germany
[2]Leibniz Institute for Baltic Sea Research Warnemünde, Rostock, Germany
[3]Private Consultant, now at Center for Global Discovery and Conservation Science, Arizona State University, Tempe, AZ 85281, USA

Correspondence: Joshua Kiesel (kiesel@geographie.uni-kiel.de)

Abstract. Hydrodynamic models are increasingly being used in recent years to map coastal floodplains on local to continental scales. On regional scales, however, high computational costs and the need for high-resolution data limit their application. Additionally, model validation constitutes a major concern, as in-situ data are hardly available or limited in spatial coverage to small parts of the study region. Here we address these challenges by developing a modelling framework, which couples a hydrodynamic coastal inundation model covering the German Baltic Sea coast with a hydrodynamic coastal ocean model of the western Baltic Sea, to produce high resolution (50 m) regional scale flood maps for the entire German Baltic Sea coast. Using a LiDAR derived digital elevation model with 1 m horizontal resolution, we derive and validate the elevation of dikes and natural flood barriers such as dunes. Using this model setup, we simulate a storm surge event from January 2019, a surge with a return period of 200 years and two sea-level rise scenarios for the year 2100 (200-year event plus 1 m and 1.5 m). We validate the simulated flood extents by comparing them to inundation maps derived from Sentinel-1 SAR satellite imagery, acquired between 1.5 and 3.5 hours after the peak of the 2019 surge, covering a large part of the study region. Our results confirm that the German Baltic Sea coast is exposed to coastal flooding, with flood extent varying between 118 km^2 and 1016 km^2 for the 2019 storm surge and a 200-year return water level plus 1.5 m of sea-level rise, respectively. Hotspots of coastal flooding are mostly located in the federal state of Mecklenburg Western Pomerania. Our results emphasise the importance of current plans to update coastal protection schemes along the German Baltic Sea coast over the course of the 21st century in order to prevent large-scale damage in the future.

1 Introduction

Sea-level rise (SLR) will increase the frequency and intensity of extreme water levels thus increasing the risk of coastal flooding with potentially far-reaching socio-economic impacts (Kirezci et al., 2020; Hinkel et al., 2014). In the European Union,

https://doi.org/10.5194/nhess-2022-275
Preprint. Discussion started: 6 January 2023


Natural Hazards and Earth System Sciences
Discussions

100,000 people are already exposed to annually flooding, and average annual flood damages are estimated to 1.4 billion €. These numbers are likely to increase until the end of the century (Vousdoukas et al., 2020). Across Europe, the Baltic and the North Sea are projected to experience the highest increase in extreme sea levels (ESL) towards the end of the century (Vousdoukas et al., 2017). In the Baltic Earth Assessment Reports (BEAR), Rutgersson et al. (2022) suggest that Germany, among other Baltic nations, will likely suffer severe damages from increased coastal flooding due to climate change. Facing a growing demand for flood risk assessments on regional scales, a better understanding of the consequences of natural hazards such as storm surges is required. Such assessments can enable society and decision makers to invest selectively in adaptation options and support policy-making (Vousdoukas et al., 2018; Rutgersson et al., 2022). The detailed mapping of coastal flood plains is a key component in improving our understanding of the impacts of SLR and ESL. High-quality inundation maps including information on flood depth and extent are critical for coastal impact assessments since the density of valuable assets often tends to increase towards the coast (Vousdoukas et al., 2016). This need has also been identified by European legislation: since 2007 the EU Flood Directive (Directive 2007/60/EC) requires member states to identify and map areas, assets and populations at risk from flooding along coastlines and water courses and to take measures to reduce flood risk. For this purpose, the Directive obliges member states to produce high quality inundation maps that account for ESL, SLR and the temporal evolution of surges.

In the Baltic Sea, ESL occur on various spatio-temporal scales and all phenomena contributing to ESL are generated mainly through meteorological and, to a limited extent, astronomical factors (Weisse and Hünicke, 2019). The most important contributions to extreme water levels come from storm surges, wind waves, and *preconditioning*, the latter of which leads to increased water volumes in the Baltic Sea before the onset of a storm (Weisse et al., 2021; Suursaar et al., 2006; Madsen et al., 2015). Due to the microtidal regime, storm surges can stay comparatively long, ranging from several hours to almost a day (Wolski and Wiśniewski, 2020).

Oceanographic forcings determining flood characteristics are the magnitude of the surge (i.e. the peak water level), the duration of the surge (particularly in the Baltic Sea), and wave setup (Höffken et al., 2020; Hendry et al., 2019). Besides the oceanographic forcings, detailed data on coastal morphology including anthropogenic flood barriers such as dikes (Leszczyńska et al., 2022; Vousdoukas et al., 2018) are important for estimating the characteristics of coastal flooding. However, data availability is often a major concern. Even if data of good quality exists for a specific region, modelling coastal flood plains on a regional scale is computationally expensive, often leading to the application of simplified, static bathtub models in coastal flood impact assessments. The bathtub model maps all coastal areas hydrologically connected to the sea below a certain (extreme) water level as inundated, without accounting for the alteration of flow as a consequence of varying surface roughness or the temporal evolution of the surge (e.g. duration). Even though these models may perform well depending on the geomorphic setting (Kumbier et al., 2017), several recent studies have pointed out that the bathtub model can overestimate coastal floodplains (Vousdoukas et al., 2016; Lopes et al., 2022; Didier et al., 2019).

https://doi.org/10.5194/nhess-2022-275
Preprint. Discussion started: 6 January 2023


Natural Hazards and Earth System Sciences Discussions

Due to the drawbacks of static inundation models, more complex, hydrodynamic models are increasingly used to map coastal flood plains on local to continental scales (Vousdoukas et al., 2016; Lopes et al., 2022; Didier et al., 2019; Bates et al., 2021). However, the application of such models is complex, sensitive to the model setup (parameterisation of surface roughness, solvers etc.) and computationally demanding, particularly when modelling at higher resolutions. This constitutes a dilemma, as the quality of regional scale assessments can be affected from coarse resolutions, which result in inaccuracies associated with the representation of the elevations of natural and anthropogenic flood barriers such as beach ridges, dunes, seawalls or dikes. In addition, comprehensive datasets on the location and characteristics of coastal protection infrastructure are missing for many parts of the world. In this context, Vousdoukas et al. (2018) highlight the urgent need for broad-scale but high detail datasets of coastal protection standards. Additional uncertainty arises from lacking data to validate modelled flood extents, the extrapolation of return water levels beyond the length of tide gauge records and the projections of future sea levels (Vousdoukas et al., 2016, 2018).

Model validation is one of the major challenges in coastal flood risk analysis as it generates awareness of model limitations. Recent advances in the application of hydrodynamic models for flood impact assessments have not been matched by advances in model validation (Rollason et al., 2018); in particular, the lack of validation data of appropriate spatial and temporal coverage constitutes a major problem (Molinari et al., 2019). For instance, studies that have modelled on global to continental scales have validated floodplains with data covering only a very small part of the entire study region (Vousdoukas et al., 2016; Sampson et al., 2015).

Here we address these challenges by developing a new modelling framework to produce high resolution (50 m) regional scale flood maps for the German Baltic Sea coast. We present a novel model setup, where we offline-couple a hydrodynamic coastal inundation model with a hydrodynamic coastal ocean model covering the western Baltic Sea, the latter of which produces spatially varying boundary conditions for the coastal inundation model. Using this setup, we perform four storm surge simulations representing 1) a 200-year event, 2) a 200-year event plus 1 m and 3) 1.5 m of SLR and 4) a simulation of the storm surge that occurred on 2nd January 2019. We used the 2019 storm surge to validate water levels produced with the coastal ocean model and the flood extent produced by the coastal inundation model. We compare flood maps derived from our coastal inundation model with floodplains generated from Sentinel-1 Synthetic Aperture Radar (SAR) satellite imagery. These images were acquired on the same day of the surge, only a few hours after the peak. More importantly, they cover a significant part of our study area.

200-year return water levels and associated hydrographs were extrapolated using a hindcast of the coastal ocean model. The hydrographs were derived using the average surge shape for each location and are in the following used as the boundary condition for the coastal inundation model. The 200-year event is used in local coastal management to determine the design heights of coastal protection measures.

https://doi.org/10.5194/nhess-2022-275
Preprint. Discussion started: 6 January 2023


Natural Hazards and Earth System Sciences Discussions

Further, we account for existing coastal protection by including in our model setup detailed information on the location and elevation of natural and anthropogenic flood barriers in the study region, which we extract from a 1 m x 1 m Light Detection and Ranging (LiDAR) derived digital elevation model (DEM).

Our analysis aims at providing 1) 200-year return water levels for several locations along the German Baltic Sea coast; 2) high resolution, validated, and hydrodynamically modelled flood maps for detailed flood impact assessment in the study region and; 3) hotspots of coastal flooding.

2 Study area

The Baltic Sea constitutes a semi-enclosed, brackish water basin that is comparatively shallow (between 53 m and 55 m on average depending on dataset (Jakobsson et al., 2019)) and has its only connection to the North Sea through the Kattegat and Skagerrak (Fig. 1). The Baltic Sea is characterised by a microtidal regime, low salinity, strong stratification, and anoxic conditions in many areas (Meier et al., 2022). The German part of the Baltic Sea is located in the south-west of the sea´s catchment and comprises the federal states of Schleswig-Holstein (SH) and Mecklenburg West Pomerania (MP) (Fig. 1). The coastal length of the German Baltic Sea is approximately 2538 km, of which 649 km are located in SH and 1889 km in MP (van der Pol et al., 2021). The German Baltic Sea coast is characterised by fjords, lagoons, islands, beaches, and soft cliffs.

The German Baltic Sea experiences storm surges mostly during strong easterly winds. The highest surge to date occurred in 1872, reaching peak water levels between 2.4 and 3.4 m above the German Ordnance Datum (NHN) in the federal state of SH. In this event, 31 people died and 15,000 lost their homes. The 1872 surge was a turning point for adaptation planning along the German Baltic Sea coast, resulting in new design standards for embankment constructions in the aftermath of the storm (Hofstede and Hamann, 2022).

Today, state embankments in SH and MP are designed to be high enough to prevent flooding during a storm surge with a return period of 200 years plus a buffer of 0.5 m to account for SLR (Melund, 2022; StALU, 2012). On the other hand, regional dikes have a variable but generally lower protection standard (Melund, 2022). During the last two decades, the concept of so called *climate dikes* has been introduced as a paradigm in embankment construction. The *climate dike* accounts for uncertainties related to SLR projections by having wider dike crests, which allows for a comparatively easy and rapid increase in dike heights without reconstructing the dike base. The *climate dike* can easily be increased in height by up to 1.5 m, and suggested extension options include 0.5 m and 1.0 m (Melund, 2022).

3 Methods and data

3.1 Overview of modelling framework and simulated scenarios

In order to simulate flood characteristics along the German Baltic Sea coast, we use a new modelling framework where we offline-couple two hydrodynamic models, a coastal ocean model (GETM) with a coastal inundation model (LISFLOOD-FP), where the coastal ocean model provides boundary conditions used to simulate coastal flood characteristics in the inundation

https://doi.org/10.5194/nhess-2022-275
Preprint. Discussion started: 6 January 2023

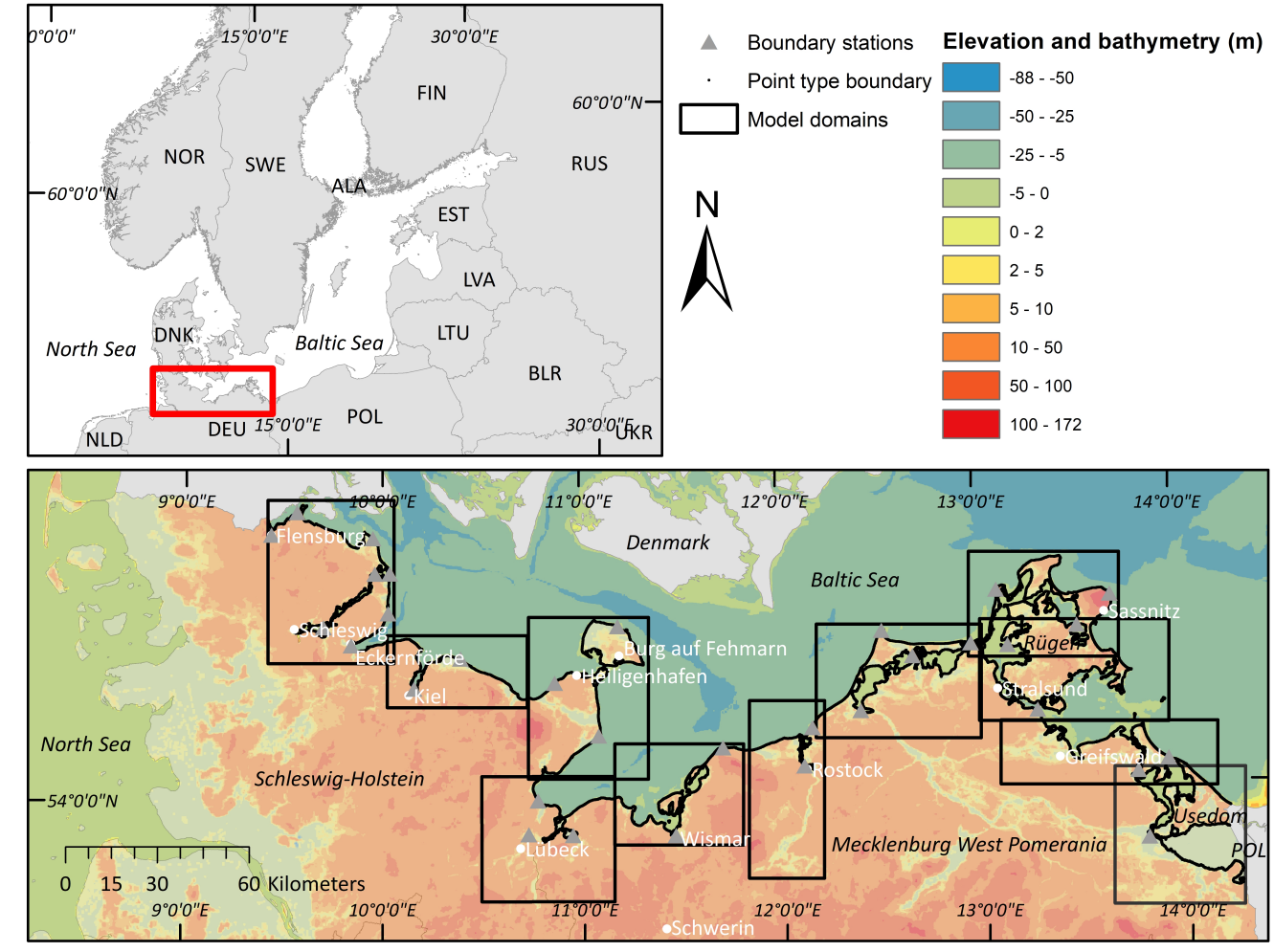

Figure 1. Top left: The Baltic Sea and its bordering nations. Bottom: The German Baltic Sea and depiction of coastal inundation model setup. Bathymetry data was taken from Baltic Sea Bathymetry Database (Helcom Secretariat) and the elevation data from Global multi-resolution terrain elevation data 2010: U.S. Geological Survey Open-File Report 2011-1073, 26 p. http://pubs.usgs.gov/of/2011/1073/, available via Helcom.

model. We use this model setup to simulate four events and scenarios: 1) The surge that occurred on 2nd January 2019, which we use to validate the coastal ocean and the inundation model. 2) A 200-year event that is used to determine the design heights of dikes along the German Baltic Sea coast. 3) The 200-year event plus 1 m of SLR and 4) a high-end scenario of the 200-year event plus 1.5 m of SLR (SLR until the year 2100). We add SLR linearly to the 200-year event (Hieronymus et al., 2018). The SLR scenarios correspond to the regional scale medium confidence projections of SSP5-8.5 (ranging between the 50th and 83rd percentile) of the latest assessment report of the Intergovernmental Panel on Climate Change (IPCC) for the tide gauges

https://doi.org/10.5194/nhess-2022-275
Preprint. Discussion started: 6 January 2023


Natural Hazards and Earth System Sciences Discussions

in Lübeck-Travemünde and Wismar (IPCC). Both sea-level rise scenarios are used in current coastal protection planning as so-called "building reserve". The building reserve allows increasing the dike heights at the end of this century by up to 1.5 m, with comparatively little effort (Melund, 2022).

3.2 Numerical setups

3.2.1 Coastal Ocean Model: GETM

The General Estuarine Transport Model (GETM, Burchard and Bolding, 2002) constitutes a structured coastal ocean model (Klingbeil et al., 2018) that solves the Reynolds averaged Navier-Stokes equations (RANS) in Boussinesq approximation. In this study, we employ it to perform a hind-cast simulation of the sea level evolution from 1961 to 2018 using its vertically integrated mode.

We employ a setup of the Western Baltic Sea in 200 m resolution based on topography obtained from the European Marine Observation and Data Network (EMODnet, https://emodnet.ec.europa.eu). As atmospheric forcing we use the HARMONIE V1 dataset (https://apps.ecmwf.int/datasets/data/uerra/) of the project 'Uncertainties in Ensembles of Regional ReAnalyses' (UERRA, https://www.uerra.eu). The wind speeds of the forcing have been increased by 7% to improve the model´s ability to match the peak water levels observed during the storm surges. The friction in the model is depth-dependent using the *law of the wall* with a roughness length of $z_0 = 5e - 05$ m. This value is smaller than usual to minimise frictional effects that may reduce the maximal surge heights in the model. The Total Variation Diminishing scheme 'Superbee' is used as the advection scheme (Pietrzak, 1998). The 200 m setup uses boundary conditions of a nesting hierarchy starting with a coarse setup of the Northwestern Atlantic Ocean (see Gräwe et al. (2015) for a detailed description of the nesting). The boundary conditions are extracted from a 1 N.m. setup of the North Sea and Baltic Sea which uses ERA5 (Hersbach et al., 2020) as atmospheric forcing. Since the UERRA data ended in 2018, the 2019 surge used here to validate the simulated flood extents is computed using the German Weather Service (DWD) forecast (Zängl et al., 2015). To keep the computation of the modelled return levels consistent to one dataset, the return level computation does not include the 2019 surge.

3.2.2 Coastal inundation model: LISFLOOD-FP

LISFLOOD-FP (here referred to as Lisflood) is a raster flood inundation model that is used to simulate fluvial or coastal flood propagation (Bates et al., 2013). Lisflood includes several solvers that simulate the propagation of the flood wave along channels and across floodplains using simplifications of the shallow water equations, making it a reduced complexity model that is a faster alternative to full shallow-water models but providing results of similar accuracy (Neal et al., 2011; Bates et al., 2013). This makes Lisflood particularly useful for large-scale inundation modelling that would otherwise be too computationally expensive (Vousdoukas et al., 2016; Bates et al., 2021).

https://doi.org/10.5194/nhess-2022-275
Preprint. Discussion started: 6 January 2023


Natural Hazards and Earth System Sciences
Discussions

3.2.3 Model setup in Lisflood

From the available solvers in Lisflood, we applied the floodplain solver "Acceleration", which is a simplified form of the shallow water equations, excluding only the convective acceleration term. The flow is calculated using "Acceleration" as a function of friction, water slopes, and local water acceleration (see Bates et al. (2013) for the respective equations). The timestep varies throughout the simulation according to the Courant-Friedrichs-Lewy condition and is related to the cell size and water depth (Bates et al., 2013).

In order to model the entire German Baltic Sea coast in 50 m resolution, we partitioned the study region into eleven model domains, each covering an area of on average 1739 km^2 (Fig. 1). Model domains were defined considering water level variability across the study region, so that each model domain is characterised by comparatively homogeneous water levels. We used a point-type boundary to force the model, whereby a boundary point was placed every 50 m along the model coastline (55,169 points in total) (Table 1). In order to account for spatial variations in water levels within each model domain, we defined a total of 32 "boundary stations" (Fig. 1), for which hydrographs were modelled in GETM for the four storm surge scenarios (2019 surge, 200-year event, 200-year event plus 1 m and 1.5 m). The boundary stations used in this study do not correspond to existing tide gauges. The modelled hydrographs were transferred from the boundary station to the nearest boundary point, which was used to force the coastal inundation model. In those cases where the nearest flood boundary station to a boundary point located on the open coast was situated inside protected fjords or lagoons or vice versa, we manually corrected that point to make sure that boundary points at the open coast are not forced with hydrographs of sheltered locations.

Model elevation and bathymetry were compiled as follows: we first aggregated the 10 m LiDAR-derived elevation data to 50 m in order to make it consistent with the bathymetry data (Table 1). Then, both datasets were merged by differentiating between sea (bathymetry) and land (elevation) areas. A resolution of 50 m is insufficient to reliably resolve natural and anthropogenic coastal protection barriers, as dike crests are typically narrower than 50 m, which is why grid sizes smaller than 10 m are recommended (Vousdoukas et al., 2012b, a). In contrast to other regional-scale studies (Vousdoukas et al., 2016), we had access to high-resolution LiDAR derived (1 x 1 m) DEMs and comprehensive datasets on the position of both state and regional dikes from local state authorities (Table 1). We used these two datasets to accurately resolve the elevation of dike crests and other anthropogenic and natural flood barriers in the 50 m elevation-bathymetry data. We integrated coastal protection measures by first extracting elevations from the 1 m x 1 m DEM within a 100 m buffer around the coastline and the dike shapes of SH and MP. We extracted maximum elevations around the coastline in order to accurately resolve natural flood barriers such as dunes and beach ridges, but to also account for a variety of hard coastal protection measures that are present in the study area, such as revetments and seawalls. The 100 m buffer was used to account for inaccuracies related to the data on dike positions and the DEM. In the next step, we aggregated these datasets to 50 m by using maximum elevations and merged them to the elevation-bathymetry data.

https://doi.org/10.5194/nhess-2022-275
Preprint. Discussion started: 6 January 2023

Natural Hazards and Earth System Sciences Discussions

Table 1. Datasets used to setup the coastal inundation model in Lisflood.

Dataset	Resolution	Source	Accuracy
Bathymetry	50 m	Federal Maritime and Hydrographic Agency (BSH)	*NA*
Elevation	10 m	ATKIS® DEM 10 (LiDAR); State Office of Geoinformation, Surveying and Cadestre MP and State Office for Suveying and Geoinformation SH	0.5 - 2.0 m
Elevation	1 m	ATKIS® DEM 1 (LiDAR); State Office of Geoinformation, Surveying and Cadestre MP and State Office for Suveying and Geoinformation SH	< 30 cm horizontally and 15 - 20 cm vertically in flat terrain
Land cover	100 m	Corine (© European Union, Copernicus Land Monitoring Service 2018, European Environment Agency (EEA))	Geometric accuracy < 100 m; Thematic accuracy > 85 %
Coastline	shapefile	(van der Pol et al., 2021)	*NA*
Dikes SH	shapefile	ATKIS®; State Office for Suveying and Geoinformation SH	The dataset contains full coverage of flood protection dikes in SH. We used the layers"rel01" and "geb03". Selected shapes are "Hochwasserdeich", "Hauptdeich", "Landesschutzdeich", "Überlaufdeich", "Leitdeich", "Schlafdeich", "Mitteldeich", "Binnendeich", "Hauptdeich 1. Deichlinie" and "2. Deichlinie".
Dikes MP	shapefile	State Office for Agriculture and the Environment Mittleres Mecklenburg, Coastal Division (internal data)	State dikes and regional dikes of water and soil associations

We estimated surface roughness by using landcover data from Corine (© European Union, Copernicus Land Monitoring Service 2018, European Environment Agency (EEA)) (Table 1) to assign Manning´s *n* coefficients. These coefficients are commonly employed for parameterising bottom friction of various land cover types in hydrodynamic simulations (Garzon and Ferreira, 2016). Since Manning´s *n* coefficients are not available for all Corine classes present in the study region, we reduced the number of classes by reclassification. The reclassification scheme is provided in Table A1 in the Appendix. We then assigned five configurations of Manning´s *n* coefficients to the remaining ten categories. In doing so, we followed the approach described in Höffken et al. (2020). First, we researched a variety of Manning´s *n* surface roughness coefficients from the literature for each of the ten land cover classes, which we then categorised into high, low and moderate values (Table 2). Some studies have used uniform Manning´s *n* coefficients or setups where the only separation in surface roughness was made

https://doi.org/10.5194/nhess-2022-275
Preprint. Discussion started: 6 January 2023

Natural Hazards and Earth System Sciences
Discussions

between land and water areas (Table 2). We have added these two setups to the configurations of Manning´s *n* coefficients that we used for model calibration (Table 2).

In this paper, model outputs (including the validation run simulating the 2019 storm surge) refer to the maximum water depth (and thus extent) predicted by the model for each pixel over the course of the simulation.

Table 2. Configuration of Manning´s *n* coefficients for selected land cover classes

Land use class	High	Low	Moderate	Uniform	Land/water
Agriculture	0.06 [1]	0.03 [3,5]	0.04 [1]	0.035 [8]	0.03 [2]
Forest	0.2 [2]	0.1 [4,5]	0.15 [3, 6, 7]	0.035 [8]	0.03 [2]
Urban	0.15 [1]	0.015 [6]	0.07 [3]	0.035 [8]	0.03 [2]
Wetland	0.08 [1]	0.035 [1]	0.06 [1]	0.035 [8]	0.03 [2]
Sea and ocean	0.03 [2]	0.012 [2]	0.02 [2]	0.035 [8]	0.02 [2]
Inland waterbodies/-courses	0.06 [2]	0.02 [2]	0.035 [2]	0.035 [8]	0.035 [2]
Green urban areas	0.12 [1]	0.035 [1,7]	0.07 [1]	0.035 [8]	0.03 [2]
Natural grasslands	0.042 [1]	0.034 [4]	0.035 [7]	0.035 [8]	0.03 [2]
Traffic	0.032 [1]	0.013 [5]	0.016 [6, 7]	0.035 [8]	0.03 [2]
Unvegetated coastal sediment	0.09 [4]	0.025 [6]	0.04 [1, 3]	0.035 [8]	0.03 [2]

[1](Bunya et al., 2010), [2](Garzon and Ferreira, 2016), [3](Wamsley et al., 2009), [4](Liu et al., 2013), [5](Papaioannou et al., 2018), [6](Hossain et al., 2009), [7](Dorn et al., 2014), [8](Liang and Smith, 2015)

3.3 Calibration of coastal inundation model

We tested the sensitivity of our model to variations in surface roughness coefficients using the different values of Manning´s *n* coefficients shown in Table 2. For this purpose, we modelled the storm surge from January 2019 and selected the three model domains that contained the largest flood plains (1, 7 and 8 from left to right in Fig. 1). The analysis showed that our model results are robust against variations in surface roughness coefficients (Table A2). In specific, variations in inundation area between highest and lowest Manning´s *n* coefficients vary between 0.09 km^2 (1.5 %, Domain 1) and 2.32 km^2 (9.5 %, Domain 7), while differences in Domain 8 amount to 1.04 km^2 (3.1 %). Variations in water depth between highest and lowest configurations in Manning´s *n* coefficients are even smaller, varying between 1 cm (Domain 1, 8) and 2 cm (Domain 7) (2.1 % and 5.1 %, respectively). Due to minor differences in flood characteristics, we employed the moderate Manning´s *n* coefficients in our model setup (Table 2).

https://doi.org/10.5194/nhess-2022-275
Preprint. Discussion started: 6 January 2023


Natural Hazards and Earth System Sciences Discussions

3.4 General Extreme Value Statistics (GEV)

To describe the distribution of ESL and return periods (RP), we used the general extreme value (GEV) distribution (Coles, 2001) using the time series of annual storm season (July to June) maxima of 30 tide gauges and 32 boundary stations (see Section 3.2.3). The GEV is defined by

$$F(t,\mu,\sigma,\xi) = \exp\left\{-\left[1+\xi\left(\frac{t-\mu}{\sigma}\right)\right]^{-1/\xi}\right\}, \tag{1}$$

where t is the sea level, μ is the location parameter, σ the scale parameter, and ξ the shape parameter. The shape parameter ξ governs the tail of the distribution and depending on its value subfamilies are defined (see also Fig. 2):

1. Gumbel distribution for $\xi \to 0$:

$$F(t,\mu,\sigma) = \exp\{-\exp\{-(t-\mu)/\sigma\}\}. \tag{2}$$

2. Fréchet distribution for $\xi > 0$:

$$F(t,\mu,\sigma,\alpha) = \begin{cases} 0 & \text{for} \quad t \le \mu, \\ \exp\left\{-\left(\frac{t-\mu}{\sigma}\right)^{-\alpha}\right\} & \text{for} \quad t > \mu. \end{cases} \tag{3}$$

3. Weibull distribution for $\xi < 0$:

$$F(t,\mu,\sigma,\alpha) = \begin{cases} \exp\left\{-\left(\frac{t-\mu}{\sigma}\right)^{\alpha}\right\} & \text{for} \quad t < \mu, \\ 1 & \text{for} \quad t \ge \mu. \end{cases} \tag{4}$$

For each gauge and boundary station used in this study, the GEV is fitted against the time series of the annual storm season's maximum. In this study we use the python code of Reinert et al. (2021) for the fitting. Using this model, we extrapolated 200-year return water levels for each tide gauge and boundary station (Fig. 2).

In order to be able to use the 200-year event as boundary condition for the coastal inundation model, we extracted the mean surge hydrograph from a hindcast between 1961 and 2018 for each boundary station and stretched the hydrograph to the corresponding 200-year return water level (see Appendix A). These 200-year events were than passed on to the coastal inundation model.

3.5 Data used for model validation

3.5.1 Tide gauge data to validate coastal ocean model

To evaluate the coastal ocean model's performance, we compare the modelled ESL to tide gauge observations, listed in Tab. 3. The gauge data is obtained from the European Marine Observation and Data Network (EMODnet, https://emodnet.ec.europa.eu). In Section 4.1 we compare the model's capability of recreating observed ESL (30 year return water level) and its ability to extrapolate 200-year return levels. We have used the full record length of each tide gauge, which is often longer than the simulation period. From each gauge, SLR has been removed by subtracting a linear fit of the time series.

https://doi.org/10.5194/nhess-2022-275
Preprint. Discussion started: 6 January 2023

Natural Hazards and Earth System Sciences
Discussions

Table 3. Overview of the gauges, their record lengths, and location used in this study. We defined gaps as missing data in the time series of greater than one day. The data is obtained from the European Marine Observation and Data Network (EMODnet, https://emodnet.ec.europa.eu).

station	record lengths	lon / lat	number of gaps
Althagen	1953-11-01 to 2020-12-31	12.42 / 54.37	3
Barhoeft	1954-11-01 to 2020-12-31	13.03 / 54.43	1
Barseback	1982-04-26 to 2020-12-31	12.90 / 55.76	None
Eckernfoerde	1989-11-01 to 2020-12-31	9.84 / 54.47	3
Flensburg	1954-11-01 to 2020-12-25	9.43 / 54.79	4
Gedser	1891-09-01 to 2020-12-31	11.93 / 54.57	None
Greifswald	1963-11-01 to 2020-12-31	13.45 / 54.09	None
Heiligenhafen	1989-06-01 to 2020-12-31	11.01 / 54.37	6
Hornbaek	1891-01-01 to 2020-12-31	12.46 / 56.09	None
Kappeln	1991-11-01 to 2020-12-31	9.94 / 54.66	None
KielHoltenau	1964-11-01 to 2020-12-31	10.16 / 54.37	None
Klagshamn	1929-11-13 to 2020-12-31	12.89 / 55.52	None
Koserow	1972-11-01 to 2019-11-13	14.00 / 54.06	9
LTKalkgrund	1990-05-01 to 2020-12-31	9.89 / 54.82	None
Langballigau	1991-11-01 to 2020-12-31	9.65 / 54.82	None
Neustadt	1991-11-01 to 2020-12-31	10.81 / 54.10	1
Rostock	1968-11-01 to 2020-12-31	12.15 / 54.08	2
Sassnitz	1954-08-01 to 2020-12-31	13.64 / 54.51	None
SchleimundeSP	1990-11-01 to 2020-12-31	10.04 / 54.67	None
Schleswig	1991-11-01 to 2020-12-31	9.57 / 54.51	None
Simrishamn	1982-05-31 to 2020-12-31	14.36 / 55.56	None
Skanor	1992-02-17 to 2020-12-31	12.83 / 55.42	None
Stralsund	1961-11-01 to 2020-12-31	13.10 / 54.32	2
Timmendorf	1961-11-01 to 2020-12-31	11.38 / 53.99	1
Travemunde	1949-11-01 to 2020-12-31	10.87 / 53.95	1
Ueckermuende	1965-11-01 to 2020-12-31	14.07 / 53.75	3
Viken	1976-04-22 to 2020-12-31	12.58 / 56.14	None
Warnemuende	1953-11-01 to 2020-12-31	12.10 / 54.17	5
Wismar	1957-11-01 to 2020-12-31	11.46 / 53.90	5
Wolgast	1965-11-01 to 2020-12-31	13.77 / 54.04	2

https://doi.org/10.5194/nhess-2022-275
Preprint. Discussion started: 6 January 2023

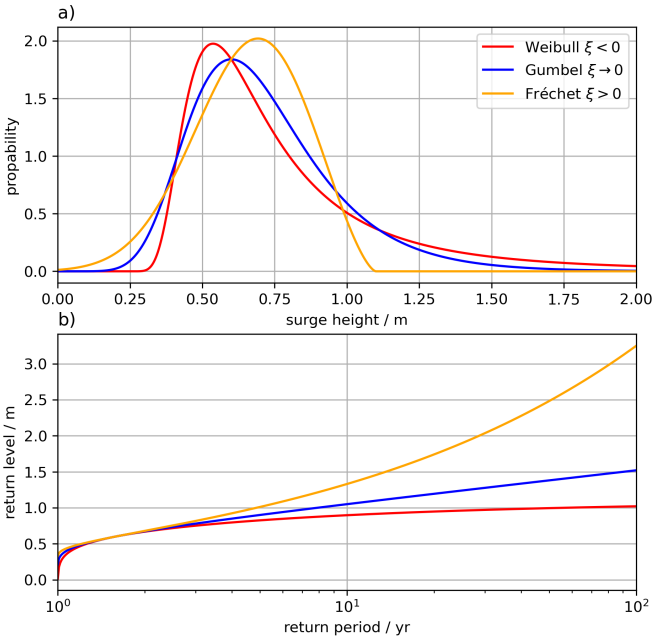

Figure 2. Visualisation of the GEV distributions (a) and the depiction of return-value plot (b), eqs. (2)-(4). The parameters for the distributions have been chosen with: $\sigma = 0.2$, $\mu = 0.6$, and $\xi = -0.4, 0, +0.4$, respectively.

3.5.2 Geodetic levelling data to validate dike heights in coastal inundation model

We used 9519 high accuracy real time kinematic (RTK) GPS points of the official dike crest geodetic levelling provided by the Schleswig-Holstein State Agency for Coastal Protection, National Park and Marine Conservation (LKN) to validate the dike heights extract from the DEM 1 (1 x 1 m horizontal resolution; Table 1). We compared the LKN RTK points and the dike crest elevations of the coastal inundation model within a 25 m buffer around the dikeline used in this study (Table 1). Next, in order to minimise errors of location (RTK points vs. 50 m x 50 m cells), we removed all cells of the coastal inundation model that were outside the value range of the geodetic dike levelling.

3.5.3 Sentinel-1 data to validate coastal inundation model

We used Sentinel-1 SAR imagery to compute the flood extent of the storm surge that occurred on January 2nd in the study area. The SAR image covers a large portion of the coastline of Schleswig-Holstein (Fig. 7) and is therefore used for evaluating the output of the coastal inundation model. SAR satellite missions enable flood extent monitoring over large geographical areas and at high spatial resolution independent of cloud coverage and illumination conditions. Specular reflectance of radar pulses at the water surface results in low return signals at-sensor, which enables delineation of water bodies from other surfaces (Clement et al., 2018). The European Space Agency's Sentinel-1 mission (S-1) offers high spatial resolution C-band SAR imagery, whereby the operation of the twin satellites S-1A and B enables observations at an increased repeat cycle of 6 days,

https://doi.org/10.5194/nhess-2022-275
Preprint. Discussion started: 6 January 2023


Natural Hazards and Earth System Sciences Discussions

which is useful for capturing short-term events. S-1B acquired the region of interest in ascending orbit and Interferometric Wide (IW) swath instrument mode on January 02, 2019 at 17:08 UTC. We used Google Earth Engine to access the calibrated and ortho-corrected Ground Range Detected (GRD) product at 10 m spatial resolution (Google Earth Engine (GEE), 2022). After visual inspection, we used VV polarisation, and applied a focal median filter with a radius of 70 m to reduce noise. We then applied a simple threshold of -16 dB to compute a binary water map, and used the shorelines of lakes, supposedly unaffected by the surge, to visually assess its suitability.

4 Results and discussion

4.1 Validation of extrapolated extreme sea levels

From the numerical simulation from 1961 to 2018, we first compared the observed and modelled ESL events with levels higher than one meter above mean sea level (Fig. 3). For each tide gauge (Tab. 3), we compute the bias and standard deviation between observed and modelled ESLs (see Fig. 3a for the station 'Kiel Holtenau' as an example). Overall, the model has a negative bias, underestimating the ESLs by 11 cm on average (Fig. 3b).

Despite the negative bias of the ESLs, the model can replicate the GEV distributions for most stations (see Fig. 4 for the station 'Kiel Holtenau' and Tab. 4 where the return levels for a 30-year event and 200-year event are listed). For 'Althagen', 'Kappeln', and 'Schleswig', the model overestimates the return levels since the lagoons are not resolved sufficiently at the resolution of 200 m. Because of the deviations in these locations, we used the tide gauge observations as input for the coastal inundation model.

For 'Barseback' and 'Viken' the model underestimates the return levels, as also seen in Fig. 3b, where 'Barseback' has the largest negative bias (note that both tide gauges are located in Sweden). The spatial distribution of the 30-year and 200-year return levels (Fig. 5) shows that the highest ESLs occur at the coasts, with ESLs decreasing from west to east. A similar pattern and return levels have been found in the literature before (e.g. Gräwe and Burchard (2012) and Wolski et al. (2014)).

4.2 Validation of dike height extraction from DEM 1

Knowledge on the elevation of dike crests constitutes a major challenge for large scale flood risk simulations as data on flood protection standards are scarce and impacts were shown to be most sensitive to variations in adaptation strategy (Hinkel et al., 2014; Vousdoukas et al., 2016; Scussolini et al., 2016). Consequently, the validation of dike heights in DEMs used to simulate coastal flooding is crucial for assessing the validity of modelled flood extents. Here we show that using high resolution (1 x 1 m) DEMs for extracting dike heights can still lead to deviations between modelled (DEM) and measured (RTK) dike crest elevations. However, we attribute the great majority of these deviations to issues related to the positioning of the raster cells extracted within the 25 m buffer around the dikeline (see Section 3.5.2). The comparison of 50 m x 50 m cells around curvy dikelines with RTK points can lead to positional errors, where cells overlaying the RTK points may represent neighbouring

https://doi.org/10.5194/nhess-2022-275
Preprint. Discussion started: 6 January 2023

Natural Hazards and Earth System Sciences
Discussions

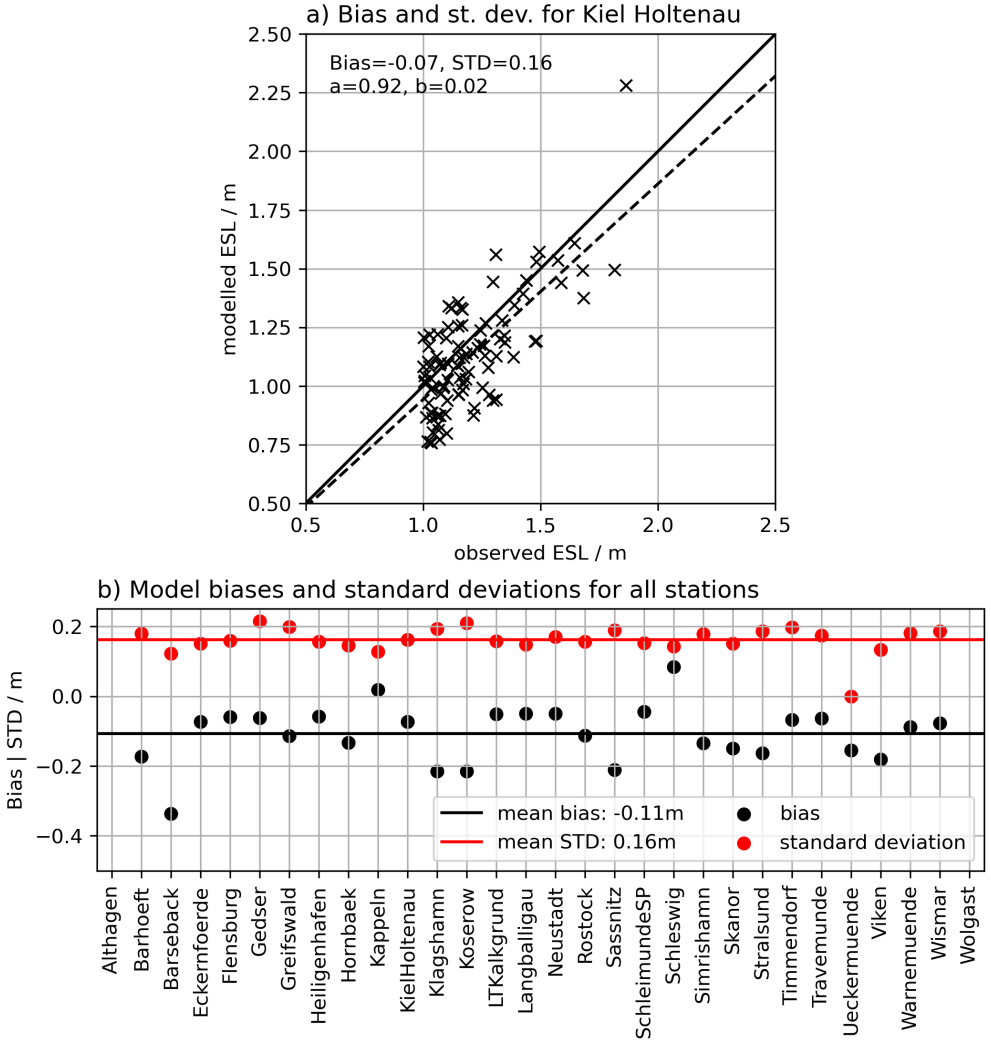

Figure 3. Validation of the hydrodynamic model's extreme sea levels exceeding 1 meter height above mean sea level. a) Comparison of the ESLs for the station 'Kiel Holtenau' in terms of bias and standard deviation (STD). The dashed line shows a linear fit where the slope denotes if the model's bias is depending on the height of the ESL. b) Summary of the biases and standard deviations for all stations. The mean bias along all stations is −11 cm, indicating that in general the ESLs are underestimated by the model. Note that no water levels above one meter are observed for the station 'Althagen' and 'Wolgast'.

https://doi.org/10.5194/nhess-2022-275
Preprint. Discussion started: 6 January 2023

Natural Hazards and Earth System Sciences
Discussions

Table 4. List of the return levels (RL) of the 30-year and 200-year return periods including the 95 % confidence intervals for different stations along the Baltic Sea coast estimated from observations (obs.) and model results (mod.).

station	obs. 30-year RL / m	mod. 30-year RL / m	obs. 200-year RL / m	mod. 200-year RL / m
Althagen	0.92 ± 0.24	1.36 ± 0.19	1.10 ± 0.36	1.71 ± 0.44
Barhoeft	1.35 ± 0.08	1.33 ± 0.10	1.44 ± 0.12	1.53 ± 0.12
Barseback	1.31 ± 0.13	0.91 ± 0.08	1.45 ± 0.19	1.00 ± 0.16
Eckernfoerde	1.69 ± 0.21	1.74 ± 0.16	1.91 ± 0.39	2.05 ± 0.28
Flensburg	1.63 ± 0.11	1.72 ± 0.16	1.80 ± 0.21	2.03 ± 0.29
Gedser	1.51 ± 0.08	1.51 ± 0.13	1.71 ± 0.11	1.74 ± 0.26
Greifswald	1.49 ± 0.12	1.49 ± 0.12	1.65 ± 0.22	1.68 ± 0.23
Heiligenhafen	1.72 ± 0.35	1.61 ± 0.17	2.15 ± 0.83	1.90 ± 0.35
Hornbaek	1.49 ± 0.06	1.43 ± 0.13	1.64 ± 0.07	1.60 ± 0.25
Kappeln	1.36 ± 0.13	1.66 ± 0.18	1.51 ± 0.23	2.01 ± 0.34
KielHoltenau	1.73 ± 0.18	1.73 ± 0.16	1.99 ± 0.36	2.03 ± 0.29
Klagshamn	1.13 ± 0.08	1.20 ± 0.11	1.27 ± 0.16	1.37 ± 0.21
Koserow	1.42 ± 0.05	1.38 ± 0.11	1.47 ± 0.07	1.56 ± 0.26
Langballigau	1.66 ± 0.26	1.69 ± 0.16	1.93 ± 0.56	1.99 ± 0.28
LTKalkgrund	1.67 ± 0.29	1.67 ± 0.15	2.03 ± 0.65	1.96 ± 0.27
Neustadt	1.64 ± 0.22	1.69 ± 0.17	1.85 ± 0.43	1.99 ± 0.33
Rostock	1.55 ± 0.19	1.52 ± 0.15	1.83 ± 0.39	1.75 ± 0.31
Sassnitz	1.22 ± 0.08	1.24 ± 0.08	1.33 ± 0.14	1.44 ± 0.13
SchleimundeSP	1.62 ± 0.24	1.69 ± 0.15	1.88 ± 0.49	1.98 ± 0.26
Schleswig	1.39 ± 0.11	1.91 ± 0.28	1.48 ± 0.21	2.44 ± 0.65
Simrishamn	1.09 ± 0.09	1.19 ± 0.11	1.19 ± 0.15	1.37 ± 0.23
Skanor	1.27 ± 0.21	1.31 ± 0.10	1.46 ± 0.44	1.48 ± 0.19
Stralsund	1.41 ± 0.13	1.39 ± 0.11	1.59 ± 0.23	1.58 ± 0.21
Timmendorf	1.65 ± 0.18	1.65 ± 0.18	1.93 ± 0.38	1.94 ± 0.38
Travemunde	1.71 ± 0.13	1.72 ± 0.18	1.92 ± 0.24	2.03 ± 0.36
Ueckermuende	1.00 ± 0.12	0.90 ± 0.13	1.15 ± 0.25	1.11 ± 0.30
Viken	1.49 ± 0.16	1.32 ± 0.13	1.69 ± 0.31	1.49 ± 0.25
Warnemuende	1.54 ± 0.16	1.50 ± 0.15	1.81 ± 0.35	1.74 ± 0.32
Wismar	1.69 ± 0.13	1.68 ± 0.19	1.89 ± 0.23	1.97 ± 0.40
Wolgast	0.96 ± 0.11	0.95 ± 0.15	1.09 ± 0.23	1.21 ± 0.40

https://doi.org/10.5194/nhess-2022-275
Preprint. Discussion started: 6 January 2023

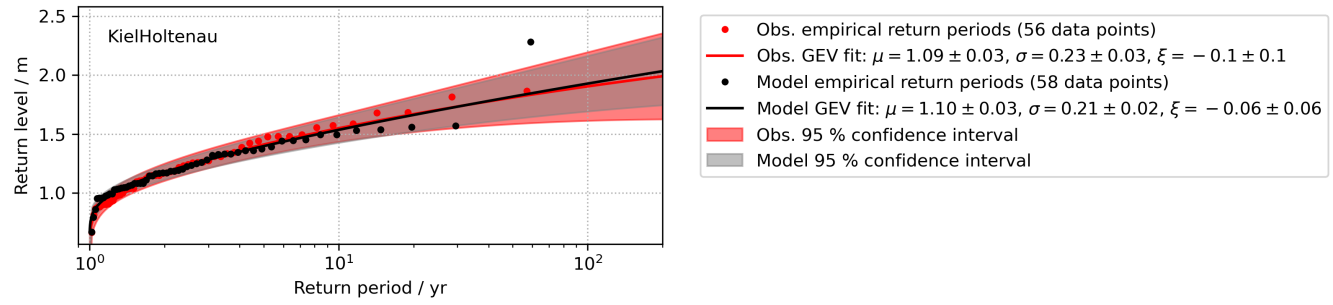

Figure 4. GEV distributions derived from the observations (red) and the model (black) for the station 'Kiel Holtenau'.

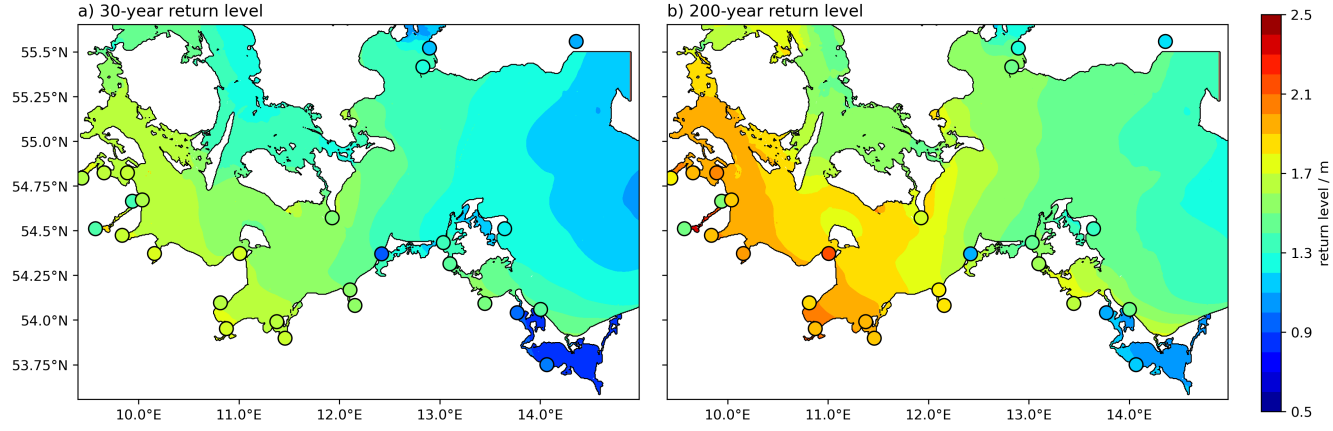

Figure 5. Modelled 30-year (a) and 200-year return levels (b) for the Western Baltic Sea. The circles denote the observed stations and values listed in Tab. 4. Note that for the 'Schlei fjord' (located between the Baltic Sea and the city of Schleswig, see (Fig. 1)), and the 'Saaler Bodden', the values are overestimated since the model has a positive bias due to the limited resolution in the lagoons, see also Tab. 4.

hills or troughs rather than the actual dikeline. This is also supported by the fact that the lowest dike heights in the coastal inundation model tend to produce higher differences when compared to the RTK measurements (and vice versa) (Fig. A2).

Given the differences in scale (points vs. 50 m x 50 m cells), we generally find that the RTK measurements and the dike heights used in the coastal inundation model are in good agreement (Fig. A3). Minimum (-2 m) and maximum deviations (3.7 m) can be substantial, while the root mean square error between both datasets is 0.65 m and the mean absolute error 0.37 m. However, 62 % of the values lie in the range between + 0.2 m and - 0.2 m difference and 77 % between - 0.5 m and + 0.5 m.

4.3 Validation of maximum sea levels during the 2nd January 2019 event

Comparing the peak water levels of the coastal ocean model with the observed maxima of the 2019 event (Fig. 6) shows that the model can capture the spatial pattern of water level variability. Overall, the model underestimates peak water levels by 5 cm on average, yet overestimates the water levels in most lagoons, as already stated in Section 4.1.

https://doi.org/10.5194/nhess-2022-275
Preprint. Discussion started: 6 January 2023

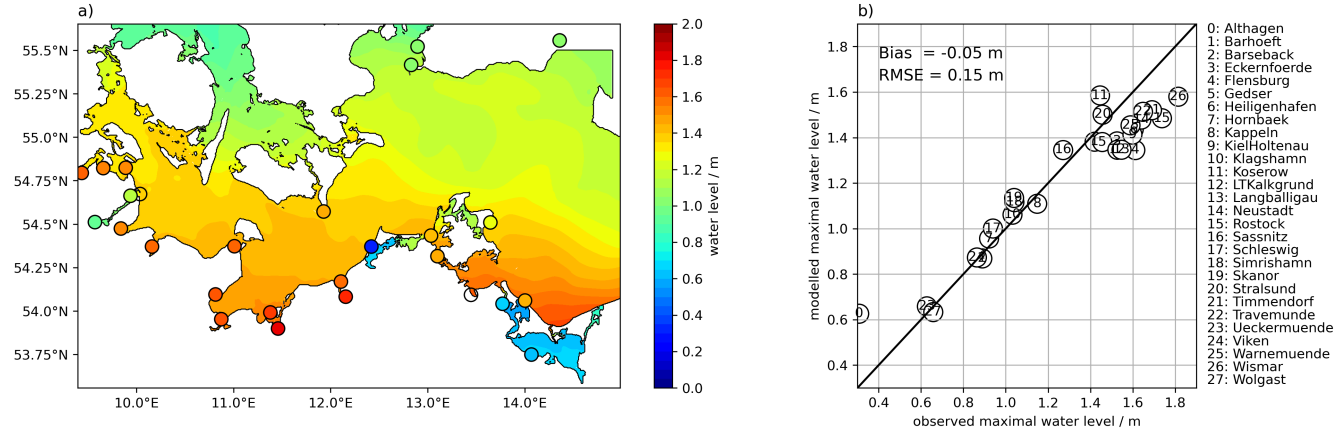

Figure 6. a) Modelled and observed maximal water levels (coloured circles) for January 2nd 2019 storm event. b) Direct comparison of the maximal water levels with the modelled maximal water levels. The bias to the observed stations is −5 cm, i.e., on average the model underestimates the maximal water levels, and the root-mean-square-error (RMSE) is 15 cm for this event.

4.4 Validation of coastal flood extents

We used the flood extent derived from S-1 SAR imagery (acquired at 17:08 UTC on the 2nd January 2019) to evaluate the validity of the coastal inundation model output. The SAR image was taken 1.5 hours after the modelled peak of the surge in Schleimünde (entrance of the Schlei fjord, which is located between the Baltic Sea and the city of Schleswig) and Timmendorf (north of Lübeck), and 3.5 hours after water levels were peaking in Kiel fjord. Only at the end of the Schlei fjord, in Schleswig, the modelled peak of the surge occurred at 23:15, more than six hours after the SAR imagery was taken. We must note that we do not consider this procedure as validation in the strict sense of the term but rather as a first-order evaluation of the model's performance. The preparation of S-1 imagery (see Section 3.5.3) and the pre-processing of elevation data (within a 100 m buffer around the coastline, each 50 m grid cell is given the maximum elevation identified in the 1 m x 1 m DEM) introduce additional uncertainties. However, we tried to account for these uncertainties by adjusting the SAR-derived and modelled floodplains prior to comparison. The flooded area was calculated as follows: first, we excluded all flooded areas inside the 100 m coastline buffer in the SAR-derived and coastal inundation model floodplains. In addition, beach lakes and lagoons cut off from the Baltic Sea via sluice gates or beach ridges (indicated by ATKIS® digital landscape model as stagnant water) were also excluded. We compared the floodplains of both datasets (SAR and coastal inundation model) by calculating the percentage of correctly predicted cells, missed cells, and overpredicted cells (Fig. 7). These indices are regularly used to assess the performance of inundation models (Vousdoukas et al., 2016; Alfieri et al., 2014). For the area covered by the SAR image (Fig. 7), the storm surge from 2nd January 2019 produced floodplains of 2.18 km^2 and 2.38 km^2 for the SAR data and the coastal inundation model, respectively. Relative to the SAR data, we calculated that 54.3 % of the inundated cells were correctly predicted, 54.5 % were overpredicted, and 26.7 % were missed. The fact that correctly predicted and missed cells do not match is caused by differences in resolution (10 m vs. 50 m for the SAR and inundation model floodplains, respectively).

https://doi.org/10.5194/nhess-2022-275
Preprint. Discussion started: 6 January 2023

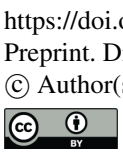

Natural Hazards and Earth System Sciences
Discussions
Open Access
EGU

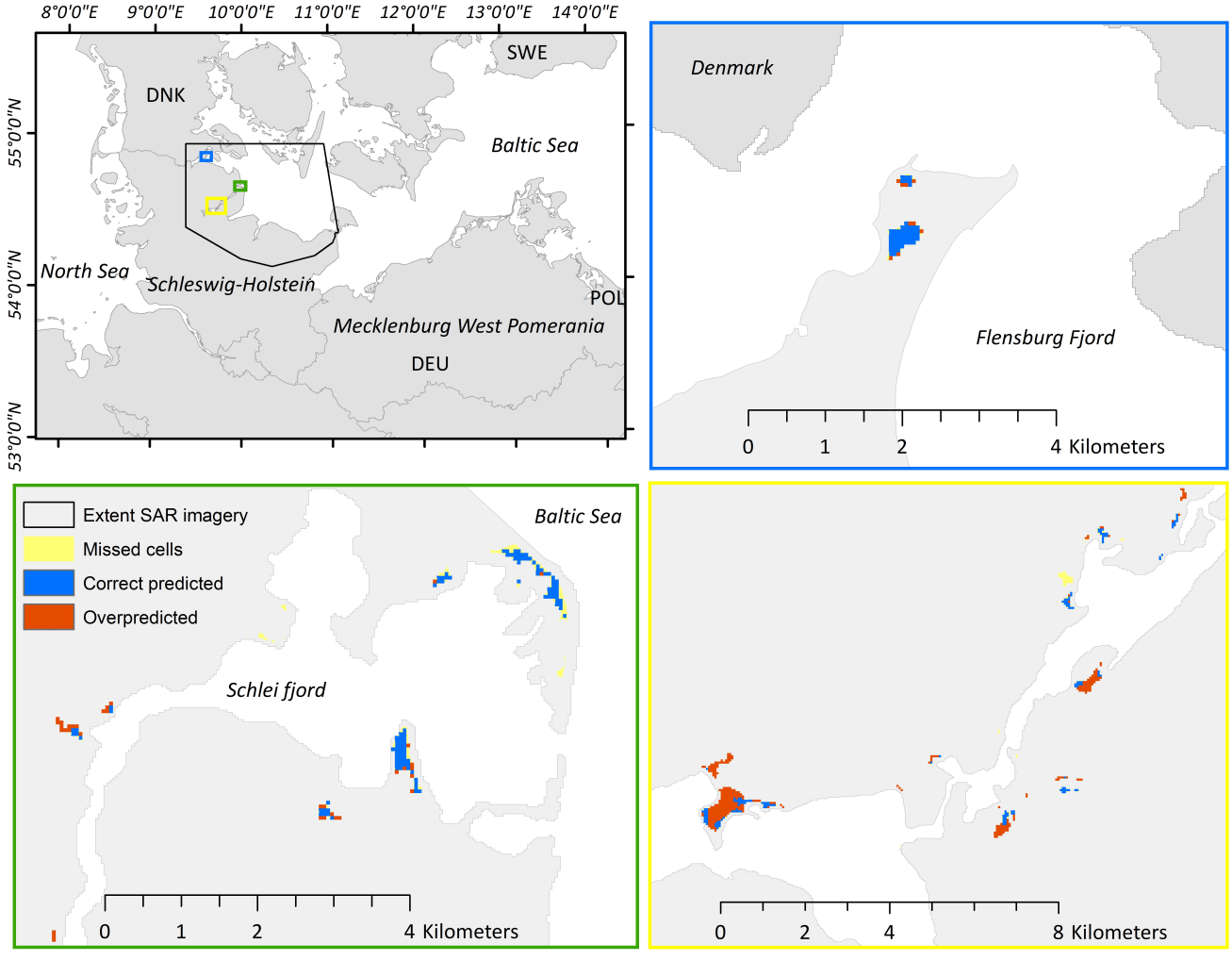

Figure 7. Example regions showing the comparison between floodplains produced with coastal inundation model and SAR data from the storm surge of January 2nd 2019

The skill indices are affected by issues related to the timing of when the SAR imagery was acquired and the decisions made concerning the preparation of SAR data. While the SAR image for most sections along the coast was acquired only a few hours after the peak of the surge (see Section 4.4), at Schleswig, located at the end of the Schlei fjord, the modelled peak of the surge occurred more than six hours after the SAR image was taken. When the SAR image was acquired, water levels at Schleswig were at 0.64 m, which is 0.35 m below the peak water level of the 2019 event at the same location (0.99 m) (see also Fig. A4 of the appendix for water level timeseries of the 2019 event for selected boundary stations).

Delineation of water surfaces from SAR imagery is based on contrast, resulting from low return signals due to specular reflectance of radar pulses at the water surface. However, this contrast decreases when backscattering increases due to wind

https://doi.org/10.5194/nhess-2022-275
Preprint. Discussion started: 6 January 2023

roughening the water surface (e.g., Twele et al., 2016; Clement et al., 2018). The amount and location of roughness depends on wind speed and direction, coastal morphology, sensor-surface geometry and polarisation, which challenges delineation based on global thresholds. The amount of backscattering may further be affected by local topography, including infrastructure and vessels, which cause high return signals and result in ports being classified as non-water. Even if water surfaces and flooded areas are well distinguishable from SAR imagery, the origin of the water seems to pose a challenge for evaluating hydrodynamic models. This is especially true if storm surges are accompanied by severe rainfall or snow melt. In addition, the closing of flood gates to prevent seaside flooding may result in accumulation of drainage water and corresponding inundation inland. At the same time, the opening of flood gates to promote flooding of certain areas during surges (e.g. for reasons of nature conservation) may result in inundation of areas which are protected by hard defences. These uncertainties can only be addressed by incorporating additional information such as operational hours of sluices and culverts. While this is particularly true for multi-temporal approaches that consider image time series, we are confident that the SAR derived flood map produced in this study is adequate to evaluate modelling outputs.

In the absence of measured *in situ* data on coastal inundation characteristics during storm surges, we propose the use of remote sensing products as a promising alternative for the validation of hydrodynamic models. Yet, the validation of SAR derived flood maps is challenging. Twele et al. (2016) and Clement et al. (2018) classified optical satellite imagery acquired on the same day as S-1 SAR imagery to validate derived flood extents. However, these studies only used one image for comparison, respectively. Hence, only a limited scope of environmental conditions potentially affecting flood mapping using SAR imagery (e.g., wind speed, rainfall) could be covered. More spatial observations are necessary to investigate the suitability of different approaches under various environmental conditions. Their collection, however, is often hampered by extreme weather conditions during storm surges at the Baltic Sea coast. Only recently, Tripathy and Malladi (2022) showed that field photographs from stationary cameras might be used for validation. Another challenge for the comparison with hydrodynamic model results is the generally short duration of ESL. Even if the latter is already quite long-lasting along the Baltic Sea coast in comparison to macrotidal environments (Wolski and Wiśniewski, 2020), the limited duration reduces the chance of suitable matchups with satellite observations. Nevertheless, the growing number of satellite missions may improve the availability of relevant observations in the future.

We believe that incorporating satellite-derived flood extents in the portfolio of potential validation data may increase opportunities to validate hydrodynamic flood models. However, such products are still dependent on algorithm development and limited by spatio-temporal coverage.

4.5 Flood characteristics of simulated storm surge scenarios

Our results confirm that the German Baltic Sea coast is exposed to coastal flooding, as a storm surge with a return period of 200-years already produces substantial inundated areas (Fig. 8, Table 5). Over the four storm surge scenarios, the majority of the flooded area is located in the federal state of MP, varying between 85 % and 89 %, whereas the contribution of SH varies between 11 % and 15 % (Table 5).

https://doi.org/10.5194/nhess-2022-275
Preprint. Discussion started: 6 January 2023

Natural Hazards and Earth System Sciences
Discussions

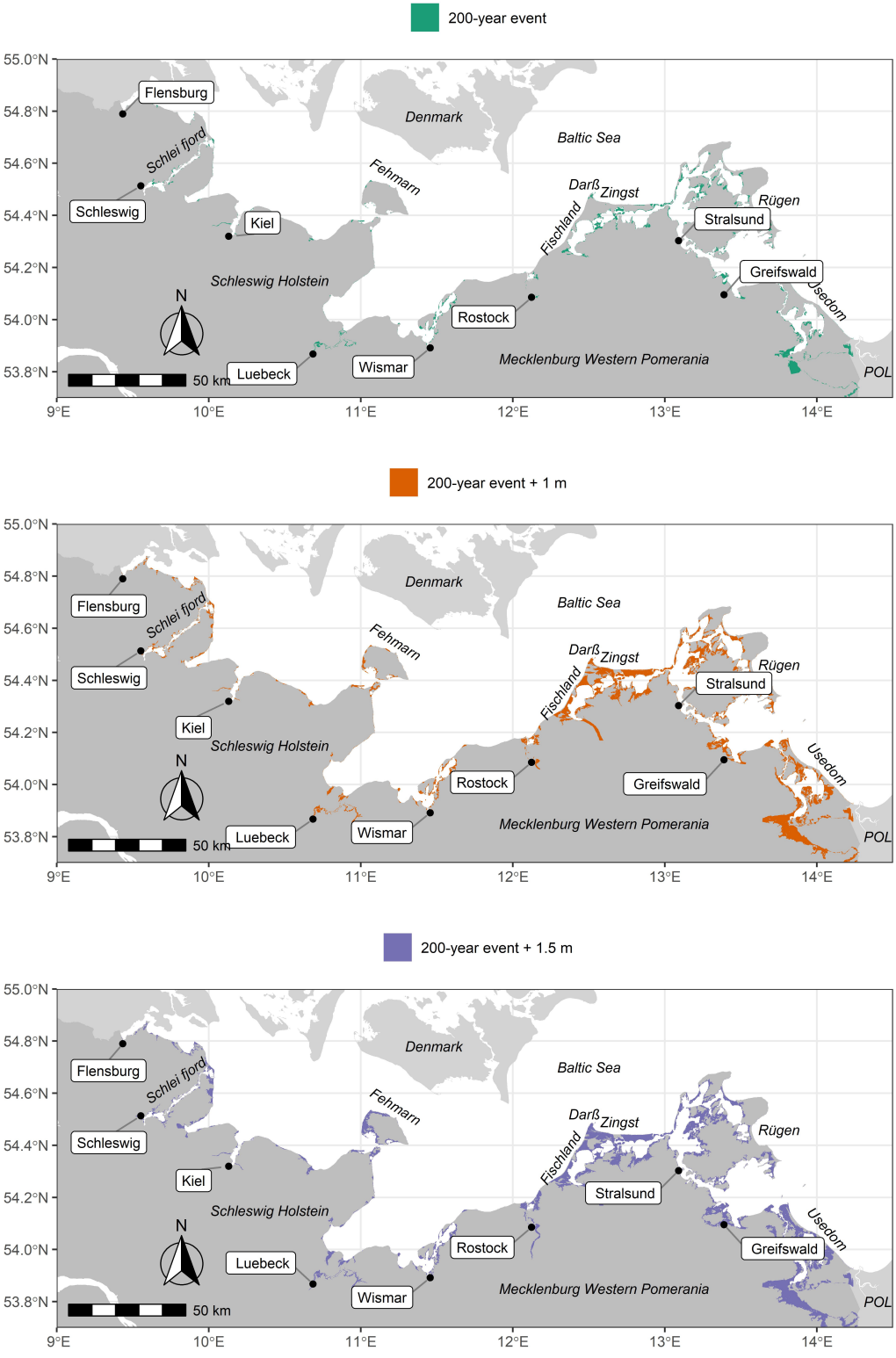

Figure 8. Floodplains for a storm surge with a return period of 200 years (top), the same surge plus 1 m sea-level rise (middle), and the same surge plus 1.5 m sea-level rise (bottom).

https://doi.org/10.5194/nhess-2022-275
Preprint. Discussion started: 6 January 2023

Natural Hazards and Earth System Sciences
Discussions

Table 5. Flood characteristics for the four storm surge scenarios for MP, SH and the entire German Baltic Sea coast.

		MP	SH	total
Storm surge 2019	flood extent km^2	101.26	16.44	117.61
	average max. flood depth (m)	0.59	0.9	0.63
200-year event	flood extent km^2	191.54	25.31	216.84
	average max. flood depth (m)	0.63	1.03	0.67
200-year event + 1 m	flood extent km^2	673.33	79.77	753.09
	average max. flood depth (m)	1.31	1.25	1.31
200-year event + 1.5 m	flood extent km^2	868.48	147.62	1016.10
	average max. flood depth (m)	1.64	1.5	1.62

In contrast to flood extent, average maximum inundation depths for the 2019 surge and the 200-year event are considerably higher in SH compared to MP (Table 5). Largest differences were found for the 200-year event, where water depths are 40 cm higher in SH. Differences converge when comparing the 200-year event with 1 m and 1.5 m of SLR. For the latter two scenarios, inundation depths are higher in MP. The analysis of flood depths during storm surges can be crucial, as it constitutes a major driver of potential flood damages to buildings and infrastructure (Merz et al., 2010; de Moel and Aerts, 2011). We believe that differences in flood depth between both states are due to variations in peak water level and coastal morphology. For the 200-year event, peak water levels are on average 0.46 m lower in MP compared to SH (2.03 m in SH and 1.57 m in MP, Table 4), potentially explaining differences in inundation depth. With respect to both SLR scenarios, we rather believe that the differences in average maximum flood depth are driven by coastal morphology.

Following Lopes et al. (2022), we show that the flood extent along the German Baltic Sea coast is highly dependent on ESL and local geomorphologic features, including anthropogenic coastal protection measures. The importance of geomorphology for inundated areas in our study region becomes evident when comparing floodplains between the federal states of SH and MP (Table 5). Despite of lower peak water levels, MP comprises much larger floodplains, which is not exclusively due to the fact that MP comprises a substantially longer coastline and thus, the potential for larger floodplains. In SH, the flood extent per km of coastline varies between 0.025 km^2 km^{-1} for the 2019 surge and 0.23 km^2 km^{-1} for the 200-year event plus 1.5 m of SLR. In contrast, the coastal length normalized flood extent in MP varies between 0.05 km^2 km^{-1} for the 2019 event and 0.46 km^2 km^{-1} for the highest surge scenario.

We find that, up from the 200-year event, the total flood extent of the German Baltic Sea coast increases linearly with rising peak water levels (Fig. 9). Between the 200-year event and the 200-year event plus 1.5 m of SLR, we calculated that a 0.5 m increase in peak water level corresponds to an increase in flood extent of 227 km^2. However, even though the average increase in peak water level across all boundary stations between the 2019 surge and the 200-year event sums up to 0.56 m, the increase in floodplain area constitutes only 99.23 km^2, clarifying that the linear increase in floodplain area is only observed above a certain threshold in peak water level (Table 5).

https://doi.org/10.5194/nhess-2022-275
Preprint. Discussion started: 6 January 2023

Natural Hazards and Earth System Sciences
Discussions

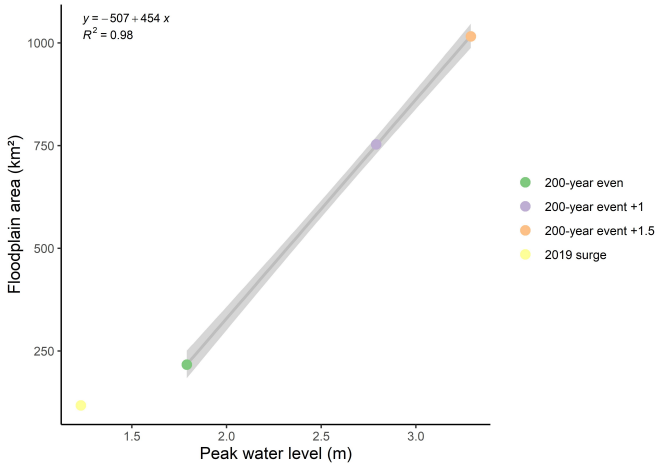

Figure 9. Correlation between floodplain area and peak water level for the 200-year event and the 200-year event plus 1 m and 1.5 m of SLR

We identify several hotspots of coastal flooding along the German Baltic Sea coast. Overall, the majority of the flood extent is located along sheltered lagoons and estuaries. In SH, hotspots are found along Flensburg fjord, the Schlei fjord, Eckernförde (domain 1), Fehmarn (domain 3) and along the Trave estuary until the city of Lübeck (domain 4). In MP, largest floodplains are identified in Rostock-Warnemünde (domain 6), Fischland-Darß-Zingst (domain 7), western and central Rügen (domains 8 and 9), north of Greifswald (domain 10), the island of Usedom and the Peene estuary, located west to the island of Usedom (domain 11). We note that most of the flooding in MP is observed inside the lagoons of Fischland-Darß-Zingst, Rügen and Usedom (Fig. 8).

4.6 Assessing the validity of the model results

To the knowledge of the authors, this study constitutes the first regional-scale assessment using a high resolution, fully validated and offline-coupled modelling framework that incorporates natural and anthropogenic flood barriers to assess extreme sea levels and associated coastal flooding along the German Baltic Sea coast. In the following, however, we discuss some limitations of our study.

Excluding waves in coastal flood modelling can lead to underestimations of flood depth and extent. A long series of breaking waves can substantially increase peak water levels due to wave setup and swash (also referred to as wave run-up) (Weisse et al., 2021; Melet et al., 2018). In studies from the Gulf of Finland and Florida, the contribution of wave setup to extreme water levels approached between 50 % and 60 % (Soomere et al., 2013; Dean and Bender, 2006), while the maximum absolute contribution to peak water levels in the previous location varied between 70 cm and 80 cm in exposed areas (Soomere et al., 2013). Even though these values should be lower in the German Baltic Sea, where recorded maximum significant wave heights are considerably lower compared to the Gulf of Finland (Alari, 2013), waves can affect coastal floodplains. This has been shown on a pan-European scale in a study by Vousdoukas et al. (2016).

https://doi.org/10.5194/nhess-2022-275
Preprint. Discussion started: 6 January 2023


Natural Hazards and Earth System Sciences Discussions

We decided in our analysis not to explicitly account for wave setup for the following reasons: first, wave setup is included in the tide gauge records that we use to extrapolate the 200-year return water levels, and for 21 of the 30 tide gauges, the coastal ocean model still overestimates the 200-year return water level. Second, there is still no conclusive information on potential changes in wave climate, and results show strong spatio-temporal variability (Weisse et al., 2021). Finally, potential wave setup along the German Baltic Sea is arguably low compared to uncertainties associated with the simulated SLR projections.

The representation of subgrid-scale coastal adaptation measures such as dikes in coastal flood modelling constitutes a major challenge that can affect simulated flood extents (Hinkel et al., 2014; Vousdoukas et al., 2016). We showed that dike crest elevations used in the coastal inundation model are generally in good agreement with high accuracy RTK measurements (see Section 4.2). However, cells that deviate substantially from overlying RTK points are present, challenging the validity of the flood extents presented here. In order to test the sensitivity of the coastal inundation model to variations in dike crest elevations, we set up the coastal inundation model using the average RTK dike height for each pixel overlaying the dikeline. Running the adjusted model for the 200-year event produced a flood extent of 27.8 km^2, being 9.8 % higher compared to the original setup (see Table 5). We therefore believe that the dike crest elevations used in the coastal inundation model are reliable. However, we must stress that in this study, we had access to high resolution elevation data, which is very rare in large scale flood modelling, suggesting that the sensitivity of most flood models against variations in dike crest elevations or elevation models in general is likely to be higher.

The results presented here do not account for morphological responses to rising water levels, such as the potential of dune collapse and dike breaching. Dike failure can occur due to hydraulic loads induced by waves and water level (Marijnissen et al., 2021) and thus, flooding behind embankments may not exclusively occur due to wave overtopping or overflow. Large-scale dike overflow is observed particularly for the 200-year event plus 1.5 m of SLR (in 2100), as dike heights in the coastal inundation model represent the status quo. The implementation of so called climate dikes in the study region, however, allows increases in dike elevation by up to 1.5 m (Melund, 2022) and further adjustments even allow adaptation for a SLR of 2.0 m (Hofstede and Hamann, 2022). Ignoring the potential of dike failure, we therefore expect that the increase in dike heights by 1.5 m may offset a large fraction of the associated rise in mean sea-level. On the other hand, the increase in dike heights will be very costly (although it is likely to be cheaper than the expected flood damage costs (Hinkel et al., 2014)) and may not be applicable to many regional dikes that are characterised by variable safety standards (Melund, 2022). Therefore, and in the light of the findings presented here, we agree that developing and identifying new and complementary measures to mitigate increasing coastal flood risks constitutes one of the most prominent challenges coastal communities are facing today (Morris et al., 2018).

5 Conclusions

We present a new, offline-coupled modeling framework to assess flood characteristics for the German Baltic Sea coast under four ESL events. We find that the largest part of the total flood extent is located in the federal state of MP. Uncertainties related to these findings are associated with the accuracy of input data (Table 1), the extreme value analysis (Table 4) and

https://doi.org/10.5194/nhess-2022-275
Preprint. Discussion started: 6 January 2023

excluded factors such as waves or the potential of dike failure (Section 4.6). We stress the importance of high resolution DEMs for extracting dike crest elevations, as the flood extents between a model where dike heights are generated from RTK measurements versus a model where we used a 1 x 1 m LiDAR dataset were found to vary by almost 10 %.

Despite the above issues, our results highlight the need to update dike heights by the end of the century, which was already initiated for state embankments years ago by the authorities with foresight (Melund, 2022; Hofstede and Hamann, 2022; StALU, 2012). Associated costs and the future of many regional dikes, which are characterised by variable design heights (Melund, 2022), remain uncertain while being dependent on the magnitude of SLR. Some could pass into the care of the federal states, but their maintenance and the necessary increase in elevation to balance high SLR scenarios (such as 1.5 m), may foster the need to rethink contemporary coastal protection measures towards new, more nature-based solutions.

In line with previous studies, we find that model validation (of all used model components) remains one of the biggest problems in large-scale flood modelling. With respect to the validation of flood extents, we show that next to the often used vertical aerial photography, other remote sensing products such as SAR-imagery may constitute a promising alternative. Even though the current available spatio-temporal resolutions still limit the use of SAR-imagery in flood model validation, the growing number of satellite missions may improve the availability of suitable observations in the future.

Data availability. The model domains, flood boundary stations, associated water level timeseries representing the four storm surge scenarios (2019 surge, 200-year event plus 1 m and 1.5 m of SLR) and the simulated flood characteristics (flood extent and depth) will be available from the KüNo data portal upon acceptance of the manuscript.

Appendix A: Construction of the 200 year event

Since we do not have any observed time series for the 200-year return water levels extrapolated with the coastal ocean model, we constructed the mean evolution of a surge for each boundary station. The resulting water level timeseries are needed as boundary condition for the coastal inundation model. Within the modelled time frame from 1961 to 2018, we extracted for each station all events exceeding a water level of one meter above mean sea level. For the stations where the water level never reached this height, we took annual maxima instead, e.g., in the lagoon Saaler Bodden. Each extracted time series has a time step of one hour. Its water level is normalised by the maximum water level of the individual event and then interpolated onto a time step of 15 min using cubic interpolation. The considered time frame starts three days before the peak water level and ends three days after the maximum water level occurrence. This allows us to compute the mean evolution of a surge by taking the mean of all events per station, see Figure A1a. Multiplying the mean, normalised evolution with the respective 200-year return level, we constructed the time series that is used as boundary condition for the coastal inundation model, see Figure A1b-f as examples.

https://doi.org/10.5194/nhess-2022-275
Preprint. Discussion started: 6 January 2023

Natural Hazards and Earth System Sciences
Discussions

Appendix Figures

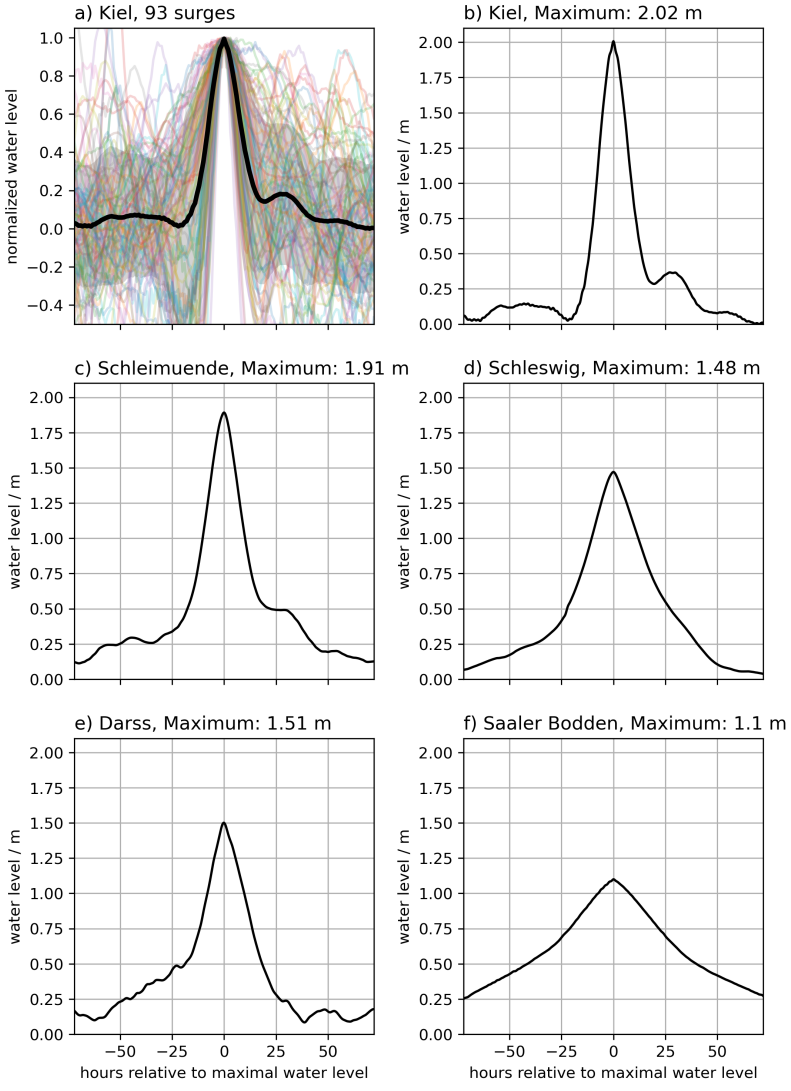

Figure A1. a) The normalised surge shape (thick black line), its standard deviation (grey area), and the individual time series (coloured) for the boundary hydrograph location 'Kiel'. b) The constructed 200-year event for the boundary hydrograph 'Kiel'. c) The constructed 200-year event for the boundary hydrograph 'Schleimuende'. d) The constructed 200-year event for the boundary hydrograph 'Schleswig'. e) The constructed 200-year event for the boundary hydrograph 'Darss'. f) The constructed 200-year event for the boundary hydrograph 'Saaler Bodden'.

Appendix Tables

https://doi.org/10.5194/nhess-2022-275
Preprint. Discussion started: 6 January 2023

Natural Hazards and Earth System Sciences
Discussions

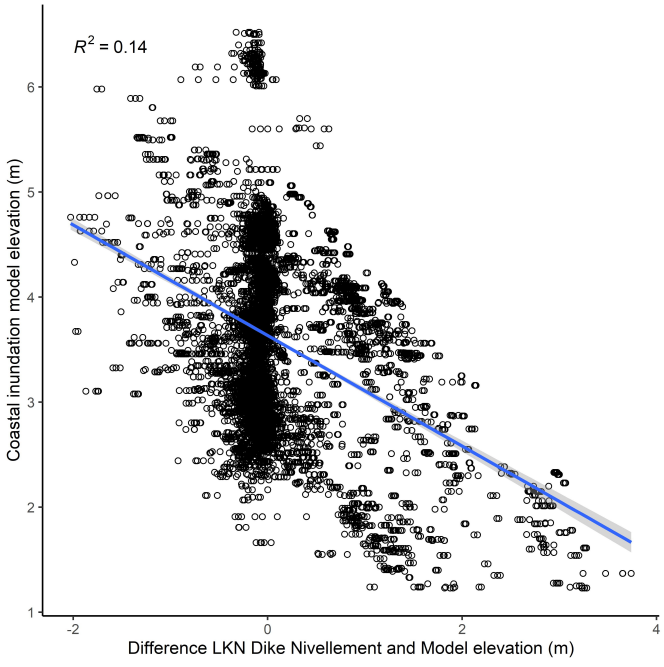

Figure A2. Correlation of dike heights of coastal inundation model and difference between geodetic dike height levelling from LKN and dike heights of coastal inundation model

https://doi.org/10.5194/nhess-2022-275
Preprint. Discussion started: 6 January 2023

Natural Hazards and Earth System Sciences
Discussions

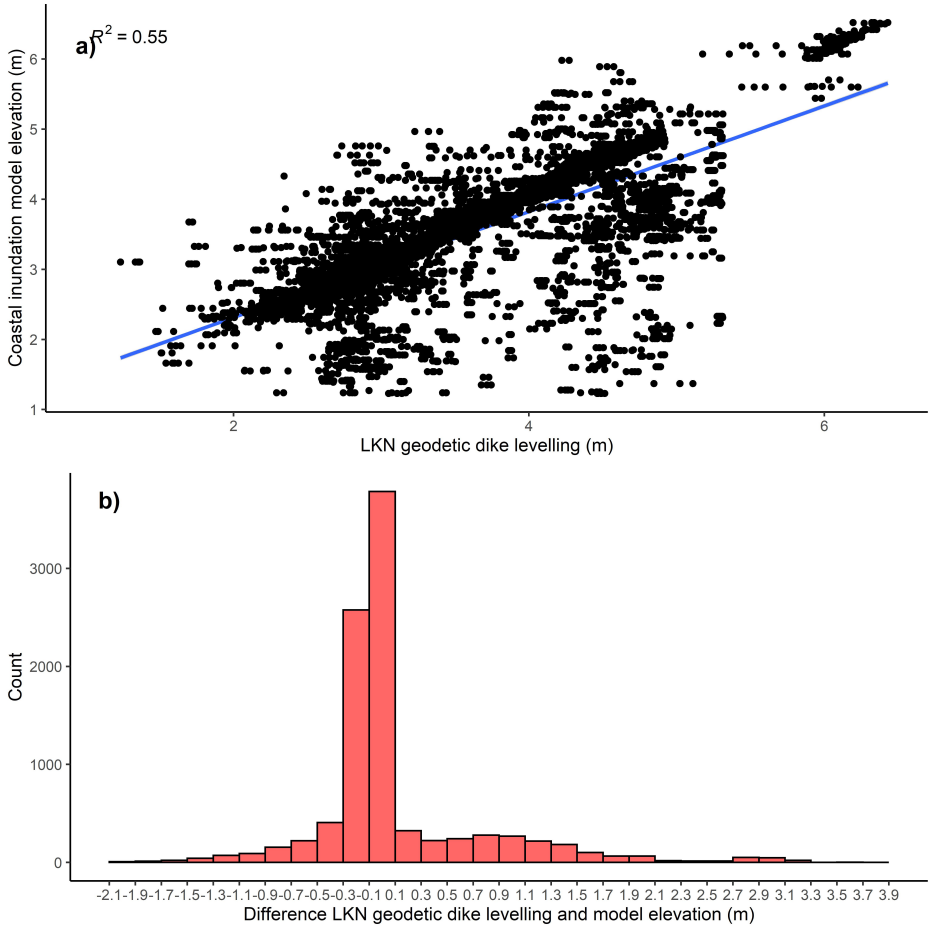

Figure A3. a) Correlation between coastal inundation model elevation and the geodetic dike levelling of the LKN.b) Histogram showing the distribution of the error between the geodetic dike levelling and the overlaying elevation of the coastal inundation model

https://doi.org/10.5194/nhess-2022-275
Preprint. Discussion started: 6 January 2023

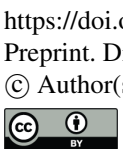

Natural Hazards and Earth System Sciences
Discussions
Open Access
EGU

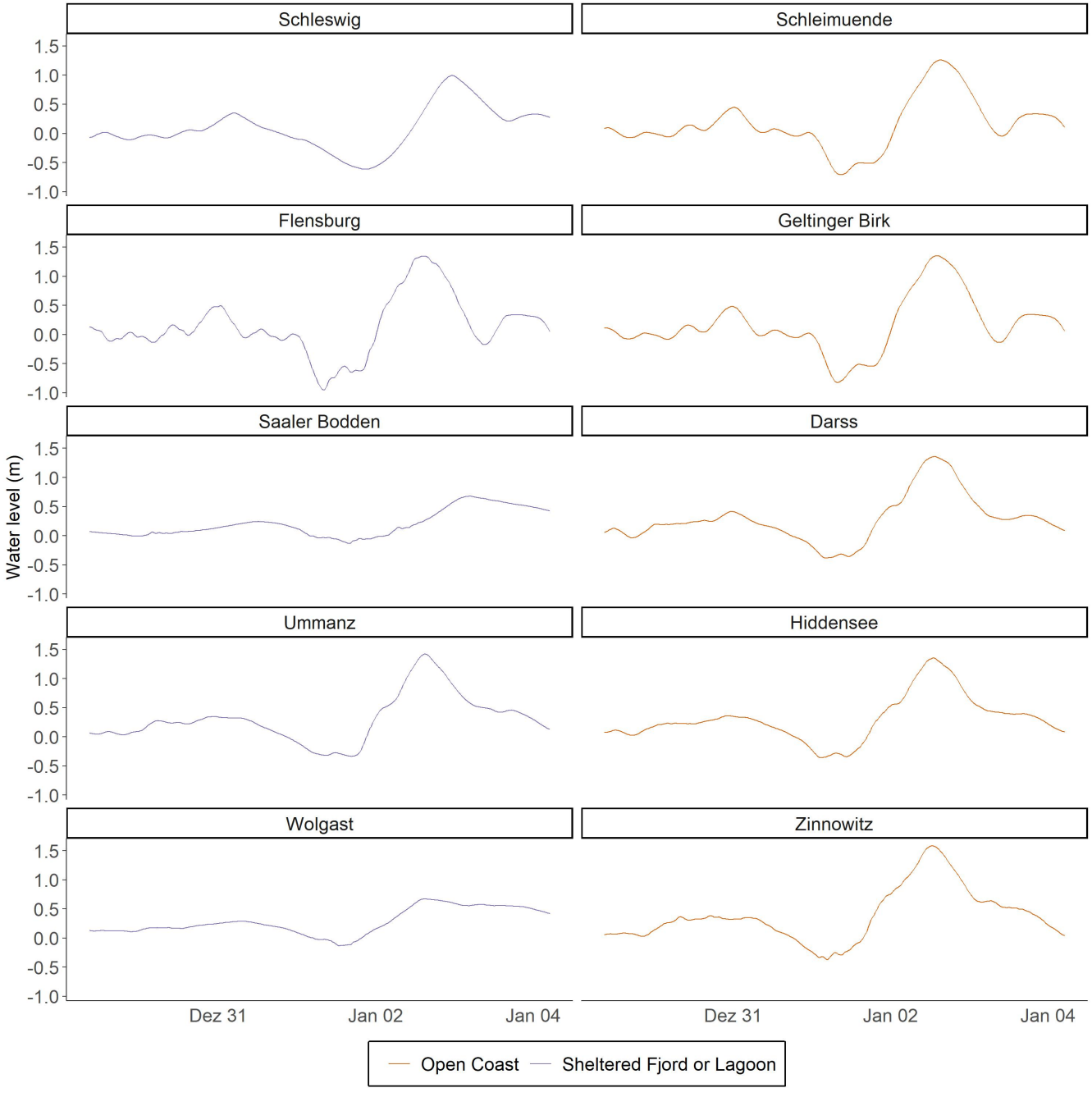

Figure A4. Water level timeseries for selected boundary stations during January 2019 storm surge

https://doi.org/10.5194/nhess-2022-275
Preprint. Discussion started: 6 January 2023

Natural Hazards and Earth System Sciences
Discussions

Table A1. Reclassification scheme of Corine land cover classes

Corine land class	New land class
continuous urban fabric	urban
discontinuous urban fabric	urban
industrial or commercial units	urban
road and railway networks and associated land	traffic
port areas	urban
airports	urban
mineral extraction sites	urban
dump sites	urban
construction sites	urban
green urban areas	green urban areas
sport and leasure facilities	green urban areas
non-irrigated arable land	agriculture
fruit tree and berry plantation	agriculture
pasture	agriculture
complex cultivation patterns	agriculture
land principally occupied by agriculture, with significant areas of natural vegetation	agriculture
broad-leaved forest	forest
coniferous forest	forest
mixed forest	forest
natural grassland	natural grassland
moors and heathland	wetland
transitional woodland-shrub	natural grassland
beaches, dunes and sand	unvegetated coastal sediment
sparsely vegetated areas	natural grassland
inland marshes	wetland
peat bog	wetland
saltmarshes	wetland
intertidal flats	unvegetated coastal sediment
water courses	inland waterbodies/courses
water bodies	inland waterbodies/courses
coastal lagoons	inland waterbodies/courses
estuaries	inland waterbodies/courses
sea and ocean	sea and ocean

https://doi.org/10.5194/nhess-2022-275
Preprint. Discussion started: 6 January 2023

Natural Hazards and Earth System Sciences
Discussions

Table A2. Flood characteristics for varying configurations of Manning´s *n* coefficients

	Domain 1		Domain 7		Domain 8	
Manning setup	**flood extent (km^2)**	**mean flood depth (m)**	**flood extent (km^2)**	**mean flood depth**	**flood extent (km^2)**	**mean flood depth (m)**
Low	5.78	0.47	24.36	0.39	33.21	0.58
High	5.69	0.46	22.04	0.37	32.17	0.57
Land/Water	5.79	0.47	24.12	0.38	33.4	0.58
Uniform	5.78	0.45	23.77	0.38	33.13	0.58
Moderate	5.73	0.46	22.84	0.38	32.58	0.58

Author contributions. JK, ATV, UG and ML designed the concept of the research. JK and ML set up the methods, ran the hydrodynamic models, analysed and plotted the results. MK processed and analysed the SAR imagery. JK wrote the manuscript with contributions from ML and MK. ATV, UG, ML and MK reviewed and edited the manuscript.

Competing interests. We declare that we have no competing interests.

Acknowledgements. JK would like to thank Dr. Jeffrey Neal (University of Bristol) and Dr. Sara Santamaria-Aguilar (University of Central Florida, previously Kiel University) for their support in setting up Lisflood. The authors would like to thank Prof. Dr. Horst Sterr (formerly Kiel University), Dr. Jacobus Hofstede (Scientific Director at Schleswig-Holstein State Government), Dr. Thomas Hirschhäuser (Head of the Hydrology Department at LKN) and Thorsten Dey (LKN) for providing helpful feedback on preliminary model outputs and fruitful discussions.

Financial support. This research is part of the ECAS-BALTIC project: Strategies of ecosystem-friendly coastal protection and ecosystem-supporting coastal adaptation for the German Baltic Sea Coast. The project is funded by the Federal Ministry of Education and Research (BMBF, funding code 03F0860H).

https://doi.org/10.5194/nhess-2022-275
Preprint. Discussion started: 6 January 2023

References

Alari, V.: Multi-Scale Wind Wave Modeling in the Baltic Sea: PhD thesis, 2013.

Alfieri, L., Salamon, P., Bianchi, A., Neal, J., Bates, P., and Feyen, L.: Advances in pan-European flood hazard mapping, Hydrological Processes, 28, 4067–4077, https://doi.org/10.1002/hyp.9947, 2014.

Bates, P., Trigg, M., Neal, J., and Dabrowa, A.: LISFLOOD-FP User manual: Code release 5.9.6, Bristol, 2013.

Bates, P. D., Quinn, N., Sampson, C., Smith, A., Wing, O., Sosa, J., Savage, J., Olcese, G., Neal, J., Schumann, G., Giustarini, L., Coxon, G., Porter, J. R., Amodeo, M. F., Chu, Z., Lewis-Gruss, S., Freeman, N. B., Houser, T., Delgado, M., Hamidi, A., Bolliger, I., McCusker, K., Emanuel, K., Ferreira, C. M., Khalid, A., Haigh, I. D., Couasnon, A., Kopp, R., Hsiang, S., and Krajewski, W. F.: Combined Modeling of US Fluvial, Pluvial, and Coastal Flood Hazard Under Current and Future Climates, Water Resources Research, 57, https://doi.org/10.1029/2020WR028673, 2021.

Bunya, S., Dietrich, J. C., Westerink, J. J., Ebersole, B. A., Smith, J. M., Atkinson, J. H., Jensen, R., Resio, D. T., Luettich, R. A., Dawson, C., Cardone, V. J., Cox, A. T., Powell, M. D., Westerink, H. J., and Roberts, H. J.: A High-Resolution Coupled Riverine Flow, Tide, Wind, Wind Wave, and Storm Surge Model for Southern Louisiana and Mississippi. Part I: Model Development and Validation, Monthly Weather Review, 138, 345–377, https://doi.org/10.1175/2009MWR2906.1, 2010.

Burchard, H. and Bolding, K.: GETM: A General Estuarine Transport Model: Scientific Documentation, European Commission, Joint Research Centre, Institute for Environment and Sustainability, https://www.io-warnemuende.de/tl_files/staff/burchard/pdf/papers/getm.pdf, 2002.

Clement, M. A., Kilsby, C. G., and Moore, P.: Multi-temporal synthetic aperture radar flood mapping using change detection, Journal of Flood Risk Management, 11, 152–168, https://doi.org/10.1111/jfr3.12303, 2018.

Coles, S.: An Introduction to Statistical Modeling of Extreme Values, Springer Series in Statistics, Springer London, London, 2001.

de Moel, H. and Aerts, J. C. J. H.: Effect of uncertainty in land use, damage models and inundation depth on flood damage estimates, Natural Hazards, 58, 407–425, https://doi.org/10.1007/s11069-010-9675-6, 2011.

Dean, R. G. and Bender, C. J.: Static wave setup with emphasis on damping effects by vegetation and bottom friction, Coastal Engineering, 53, 149–156, https://doi.org/10.1016/j.coastaleng.2005.10.005, 2006.

Didier, D., Baudry, J., Bernatchez, P., Dumont, D., Sadegh, M., Bismuth, E., Bandet, M., Dugas, S., and Sévigny, C.: Multihazard simulation for coastal flood mapping: Bathtub versus numerical modelling in an open estuary, Eastern Canada, Journal of Flood Risk Management, 12, https://doi.org/10.1111/jfr3.12505, 2019.

Dorn, H., Vetter, M., and Höfle, B.: GIS-Based Roughness Derivation for Flood Simulations: A Comparison of Orthophotos, LiDAR and Crowdsourced Geodata, Remote Sensing, 6, 1739–1759, https://doi.org/10.3390/rs6021739, 2014.

Garzon, J. and Ferreira, C.: Storm Surge Modeling in Large Estuaries: Sensitivity Analyses to Parameters and Physical Processes in the Chesapeake Bay, Journal of Marine Science and Engineering, 4, 45, https://doi.org/10.3390/jmse4030045, 2016.

Google Earth Engine (GEE): Sentinel-1 SAR GRD: C-band Synthetic Aperture Radar Ground Range Detected, log scaling, https://developers.google.com/earth-engine/datasets/catalog/COPERNICUS_S1_GRD, 2022.

Gräwe, U. and Burchard, H.: Storm surges in the Western Baltic Sea: the present and a possible future, Climate Dynamics, 39, 165–183, https://doi.org/10.1007/s00382-011-1185-z, 2012.

Gräwe, U., Naumann, M., Mohrholz, V., and Burchard, H.: Anatomizing one of the largest saltwater inflows into the B altic S ea in D ecember 2014, Journal of Geophysical Research: Oceans, 120, 7676–7697, https://doi.org/10.1002/2015JC011269, 2015.

https://doi.org/10.5194/nhess-2022-275
Preprint. Discussion started: 6 January 2023

Hendry, A., Haigh, I. D., Nicholls, R. J., Winter, H., Neal, R., Wahl, T., Joly-Laugel, A., and Darby, S. E.: Assessing the characteristics and drivers of compound flooding events around the UK coast, Hydrology and Earth System Sciences, 23, 3117–3139, https://doi.org/10.5194/hess-23-3117-2019, 2019.

Hersbach, H., Bell, B., Berrisford, P., Hirahara, S., Horányi, A., Muñoz-Sabater, J., Nicolas, J., Peubey, C., Radu, R., Schepers, D., Simmons, A., Soci, C., Abdalla, S., Abellan, X., Balsamo, G., Bechtold, P., Biavati, G., Bidlot, J., Bonavita, M., Chiara, G., Dahlgren, P., Dee, D., Diamantakis, M., Dragani, R., Flemming, J., Forbes, R., Fuentes, M., Geer, A., Haimberger, L., Healy, S., Hogan, R. J., Hólm, E., Janisková, M., Keeley, S., Laloyaux, P., Lopez, P., Lupu, C., Radnoti, G., Rosnay, P., Rozum, I., Vamborg, F., Villaume, S., and Thépaut, J.-N.: The ERA5 global reanalysis, Quarterly Journal of the Royal Meteorological Society, 146, 1999–2049, https://doi.org/10.1002/qj.3803, 2020.

Hieronymus, M., Dieterich, C., Andersson, H., and Hordoir, R.: The effects of mean sea level rise and strengthened winds on extreme sea levels in the Baltic Sea, Theoretical and Applied Mechanics Letters, 8, 366–371, https://doi.org/10.1016/j.taml.2018.06.008, 2018.

Hinkel, J., Lincke, D., Vafeidis, A. T., Perrette, M., Nicholls, R. J., Tol, R. S. J., Marzeion, B., Fettweis, X., Ionescu, C., and Levermann, A.: Coastal flood damage and adaptation costs under 21st century sea-level rise, Proceedings of the National Academy of Sciences of the United States of America, 111, 3292–3297, https://doi.org/10.1073/pnas.1222469111, 2014.

Höffken, J., Vafeidis, A. T., MacPherson, L. R., and Dangendorf, S.: Effects of the Temporal Variability of Storm Surges on Coastal Flooding, Frontiers in Marine Science, 7, https://doi.org/10.3389/fmars.2020.00098, 2020.

Hofstede, J. and Hamann, M.: The 1872 catastrophic storm surge at the Baltic Sea coast of Schleswig-Holstein; lessons learned?, Die Küste, https://doi.org/10.18171/1.092101, 2022.

Hossain, A., Jia, Y., and Chao, X.: Estimation of Manning's roughness coefficient distribution for hydrodynamic model using remotely sensed land cover features, in: 2009 17th International Conference on Geoinformatics, pp. 1–4, IEEE, https://doi.org/10.1109/GEOINFORMATICS.2009.5293484, 2009.

IPCC: Climate Change 2021: The Physical Science Basis. Contribution of Working Group I to the Sixth Assessment Report of the Intergovernmental Panel on Climate Change, doi:10.1017/9781009157896.

Jakobsson, M., Stranne, C., O'Regan, M., Greenwood, S. L., Gustafsson, B., Humborg, C., and Weidner, E.: Bathymetric properties of the Baltic Sea, Ocean Science, 15, 905–924, https://doi.org/10.5194/os-15-905-2019, 2019.

Kirezci, E., Young, I. R., Ranasinghe, R., Muis, S., Nicholls, R. J., Lincke, D., and Hinkel, J.: Projections of global-scale extreme sea levels and resulting episodic coastal flooding over the 21st Century, Scientific reports, 10, 11 629, https://doi.org/10.1038/s41598-020-67736-6, 2020.

Klingbeil, K., Lemarié, F., Debreu, L., and Burchard, H.: The numerics of hydrostatic structured-grid coastal ocean models: State of the art and future perspectives, Ocean Modelling, 125, 80–105, https://doi.org/10.1016/j.ocemod.2018.01.007, 2018.

Kumbier, K., Carvalho, R. C., Vafeidis, A. T., and Woodroffe, C. D.: Modelling inundation extents of the June 2016 storm surges in estuarine environments using static and dynamic approaches: 26th NSW Coastal Conference, Faculty of Science, Medicine and Health - Papers: part A. 5351, pp. 1–15, 2017.

Leszczyńska, K., Stattegger, K., Moskalewicz, D., Jagodziński, R., Kokociński, M., Niedzielski, P., and Szczuciński, W.: Controls on coastal flooding in the southern Baltic Sea revealed from the late Holocene sedimentary records, Scientific reports, 12, 9710, https://doi.org/10.1038/s41598-022-13860-4, 2022.

Liang, Q. and Smith, L. S.: A high-performance integrated hydrodynamic modelling system for urban flood simulations, Journal of Hydroinformatics, 17, 518–533, https://doi.org/10.2166/hydro.2015.029, 2015.

https://doi.org/10.5194/nhess-2022-275
Preprint. Discussion started: 6 January 2023

Liu, H., Zhang, K., Li, Y., and Xie, L.: Numerical study of the sensitivity of mangroves in reducing storm surge and flooding to hurricane characteristics in southern Florida, Continental Shelf Research, 64, 51–65, https://doi.org/10.1016/j.csr.2013.05.015, 2013.

Lopes, C. L., Sousa, M. C., Ribeiro, A., Pereira, H., Pinheiro, J. P., Vaz, L., and Dias, J. M.: Evaluation of future estuarine floods in a sea level rise context, Scientific reports, 12, 8083, https://doi.org/10.1038/s41598-022-12122-7, 2022.

Madsen, K. S., Høyer, J. L., Fu, W., and Donlon, C.: Blending of satellite and tide gauge sea level observations and its assimilation in a storm surge model of the N orth S ea and B altic S ea, Journal of Geophysical Research: Oceans, 120, 6405–6418, https://doi.org/10.1002/2015JC011070, 2015.

Marijnissen, R. J., Kok, M., Kroeze, C., and van Loon-Steensma, J. M.: Flood risk reduction by parallel flood defences – Case-study of a coastal multifunctional flood protection zone, Coastal Engineering, 167, 103 903, https://doi.org/10.1016/j.coastaleng.2021.103903, 2021.

Meier, H. E. M., Kniebusch, M., Dieterich, C., Gröger, M., Zorita, E., Elmgren, R., Myrberg, K., Ahola, M. P., Bartosova, A., Bonsdorff, E., Börgel, F., Capell, R., Carlén, I., Carlund, T., Carstensen, J., Christensen, O. B., Dierschke, V., Frauen, C., Frederiksen, M., Gaget, E., Galatius, A., Haapala, J. J., Halkka, A., Hugelius, G., Hünicke, B., Jaagus, J., Jüssi, M., Käyhkö, J., Kirchner, N., Kjellström, E., Kulinski, K., Lehmann, A., Lindström, G., May, W., Miller, P. A., Mohrholz, V., Müller-Karulis, B., Pavón-Jordán, D., Quante, M., Reckermann, M., Rutgersson, A., Savchuk, O. P., Stendel, M., Tuomi, L., Viitasalo, M., Weisse, R., and Zhang, W.: Climate change in the Baltic Sea region: a summary, Earth System Dynamics, 13, 457–593, https://doi.org/10.5194/esd-13-457-2022, 2022.

Melet, A., Meyssignac, B., Almar, R., and Le Cozannet, G.: Under-estimated wave contribution to coastal sea-level rise, Nature Climate Change, 8, 234–239, https://doi.org/10.1038/s41558-018-0088-y, 2018.

Melund: Generalplan Küstenschutz des Landes Schleswig-Holstein: Fortschreibung 2022, Kiel, https://www.schleswig-holstein.de/DE/fachinhalte/K/kuestenschutz/Downloads/Generalplan.pdf?__blob=publicationFile&v=2, 2022.

Merz, B., Kreibich, H., Schwarze, R., and Thieken, A.: Review article "Assessment of economic flood damage", Natural Hazards and Earth System Sciences, 10, 1697–1724, https://doi.org/10.5194/nhess-10-1697-2010, 2010.

Molinari, D., de Bruijn, K. M., Castillo-Rodríguez, J. T., Aronica, G. T., and Bouwer, L. M.: Validation of flood risk models: Current practice and possible improvements, International Journal of Disaster Risk Reduction, 33, 441–448, https://doi.org/10.1016/j.ijdrr.2018.10.022, 2019.

Morris, R. L., Konlechner, T. M., Ghisalberti, M., and Swearer, S. E.: From grey to green: Efficacy of eco-engineering solutions for nature-based coastal defence, Global change biology, 24, 1827–1842, https://doi.org/10.1111/gcb.14063, 2018.

Neal, J., Schumann, G., Fewtrell, T., Budimir, M., Bates, P., and Mason, D.: Evaluating a new LISFLOOD-FP formulation with data from the summer 2007 floods in Tewkesbury, UK, Journal of Flood Risk Management, 4, 88–95, https://doi.org/10.1111/j.1753-318X.2011.01093.x, 2011.

Papaioannou, G., Efstratiadis, A., Vasiliades, L., Loukas, A., Papalexiou, S., Koukouvinos, A., Tsoukalas, I., and Kossieris, P.: An Operational Method for Flood Directive Implementation in Ungauged Urban Areas, Hydrology, 5, 24, https://doi.org/10.3390/hydrology5020024, 2018.

Pietrzak, J.: The Use of TVD Limiters for Forward-in-Time Upstream-Biased Advection Schemes in Ocean Modeling, Monthly Weather Review, 126, 812–830, https://doi.org/10.1175/1520-0493(1998)126<0812:TUOTLF>2.0.CO;2, 1998.

Reinert, M., Pineau-Guillou, L., Raillard, N., and Chapron, B.: Seasonal Shift in Storm Surges at Brest Revealed by Extreme Value Analysis, Journal of Geophysical Research: Oceans, 126, https://doi.org/10.1029/2021JC017794, 2021.

Rollason, E., Bracken, L. J., Hardy, R. J., and Large, A.: The importance of volunteered geographic information for the validation of flood inundation models, Journal of Hydrology, 562, 267–280, https://doi.org/10.1016/j.jhydrol.2018.05.002, 2018.

https://doi.org/10.5194/nhess-2022-275
Preprint. Discussion started: 6 January 2023

Rutgersson, A., Kjellström, E., Haapala, J., Stendel, M., Danilovich, I., Drews, M., Jylhä, K., Kujala, P., Larsén, X. G., Halsnæs, K., Lehtonen, I., Luomaranta, A., Nilsson, E., Olsson, T., Särkkä, J., Tuomi, L., and Wasmund, N.: Natural hazards and extreme events in the Baltic Sea region, Earth System Dynamics, 13, 251–301, https://doi.org/10.5194/esd-13-251-2022, 2022.

Sampson, C. C., Smith, A. M., Bates, P. D., Neal, J. C., Alfieri, L., and Freer, J. E.: A high-resolution global flood hazard model, Water Resources Research, 51, 7358–7381, https://doi.org/10.1002/2015WR016954, 2015.

Scussolini, P., Aerts, J. C. J. H., Jongman, B., Bouwer, L. M., Winsemius, H. C., de Moel, H., and Ward, P. J.: FLOPROS: an evolving global database of flood protection standards, Natural Hazards and Earth System Sciences, 16, 1049–1061, https://doi.org/10.5194/nhess-16-1049-2016, 2016.

Soomere, T., Pindsoo, K., Bishop, S. R., Käärd, A., and Valdmann, A.: Mapping wave set-up near a complex geometric urban coastline, Natural Hazards and Earth System Sciences, 13, 3049–3061, https://doi.org/10.5194/nhess-13-3049-2013, 2013.

StALU: Regelwerk Küstenschutz Mecklenburg-Vorpommern: Küstenraum und Bemessungsgrößen von Küstenschutzanlagen in M-V, Verlag Redieck & Schade GmbH, Rostock, 2012.

Suursaar, Ü., Kullas, T., Otsmann, M., Saaremäe, I., Kuik, J., and Merilain, M.: Cyclone Gudrun in January 2005 and modelling its hydrodynamic consequences in the Estonian coastal waters, Boreal Environment Research, 11, 143–159, 2006.

Tripathy, P. and Malladi, T.: Global Flood Mapper: a novel Google Earth Engine application for rapid flood mapping using Sentinel-1 SAR, Natural Hazards, https://doi.org/10.1007/s11069-022-05428-2, 2022.

Twele, A., Cao, W., Plank, S., and Martinis, S.: Sentinel-1-based flood mapping: a fully automated processing chain, International Journal of Remote Sensing, 37, 2990–3004, https://doi.org/10.1080/01431161.2016.1192304, 2016.

van der Pol, T., Hinkel, J., Merkens, J., MacPherson, L., Vafeidis, A. T., Arns, A., and Dangendorf, S.: Regional economic analysis of flood defence heights at the German Baltic Sea coast: A multi-method cost-benefit approach for flood prevention, Climate Risk Management, 32, 100 289, https://doi.org/10.1016/j.crm.2021.100289, 2021.

Vousdoukas, M., Mentaschi, L., Mongelli, I., Martinez, C., Hinkel, J., Ward, P., Gosling, S., and Feyen, L.: Adapting to rising coastal flood risk in the EU under climate change, EUR 29969 EN, Publications Office of the European Union, Luxembourg, doi:10.2760/456870, 2020.

Vousdoukas, M. I., Almeida, L. P. M., and Ferreira, Ó.: Beach erosion and recovery during consecutive storms at a steep-sloping, meso-tidal beach, Earth Surface Processes and Landforms, 37, 583–593, https://doi.org/10.1002/esp.2264, 2012a.

Vousdoukas, M. I., Ferreira, Ó., Almeida, L. P., and Pacheco, A.: Toward reliable storm-hazard forecasts: XBeach calibration and its potential application in an operational early-warning system, Ocean Dynamics, 62, 1001–1015, https://doi.org/10.1007/s10236-012-0544-6, 2012b.

Vousdoukas, M. I., Voukouvalas, E., Mentaschi, L., Dottori, F., Giardino, A., Bouziotas, D., Bianchi, A., Salamon, P., and Feyen, L.: Developments in large-scale coastal flood hazard mapping, Natural Hazards and Earth System Sciences, 16, 1841–1853, https://doi.org/10.5194/nhess-16-1841-2016, 2016.

Vousdoukas, M. I., Mentaschi, L., Voukouvalas, E., Verlaan, M., and Feyen, L.: Extreme sea levels on the rise along Europe's coasts, Earth's Future, 5, 304–323, https://doi.org/10.1002/2016EF000505, 2017.

Vousdoukas, M. I., Bouziotas, D., Giardino, A., Bouwer, L. M., Voukouvalas, E., Mentaschi, L., and Feyen, L.: Understanding epistemic uncertainty in large-scale coastal flood risk assessment for present and future climates, Natural Hazards and Earth System Sciences, pp. 2127–2142, https://doi.org/10.5194/nhess-18-2127-2018, 2018.

Wamsley, T. V., Cialone, M. A., Smith, J. M., Ebersole, B. A., and Grzegorzewski, A. S.: Influence of landscape restoration and degradation on storm surge and waves in southern Louisiana, Natural Hazards, 51, 207–224, https://doi.org/10.1007/s11069-009-9378-z, 2009.

https://doi.org/10.5194/nhess-2022-275
Preprint. Discussion started: 6 January 2023

Weisse, R. and Hünicke, B.: Baltic Sea Level: Past, Present, and Future, in: Oxford Research Encyclopedia of Climate Science, Oxford University Press, Oxford, https://doi.org/10.1093/acrefore/9780190228620.013.693, 2019.

Weisse, R., Dailidienė, I., Hünicke, B., Kahma, K., Madsen, K., Omstedt, A., Parnell, K., Schöne, T., Soomere, T., Zhang, W., and Zorita, E.: Sea level dynamics and coastal erosion in the Baltic Sea region, Earth System Dynamics, 12, 871–898, https://doi.org/10.5194/esd-12-871-2021, 2021.

Wolski, T. and Wiśniewski, B.: Geographical diversity in the occurrence of extreme sea levels on the coasts of the Baltic Sea, Journal of Sea Research, 159, 101 890, https://doi.org/10.1016/j.seares.2020.101890, 2020.

Wolski, T., Wiśniewski, B., Giza, A., Kowalewska-Kalkowska, H., Boman, H., Grabbi-Kaiv, S., Hammarklint, T., Holfort, J., and Lydeikaitė, Ž.: Extreme sea levels at selected stations on the Baltic Sea coast, Oceanologia, 56, 259–290, https://doi.org/10.5697/oc.56-2.259, 2014.

Zängl, G., Reinert, D., Rípodas, P., and Baldauf, M.: The ICON (ICOsahedral Non-hydrostatic) modelling framework of DWD and MPI-M: Description of the non-hydrostatic dynamical core, Quarterly Journal of the Royal Meteorological Society, 141, 563–579, https://doi.org/10.1002/qj.2378, 2015.